NASA TECHNICAL NOTE

NASA TN D-3797

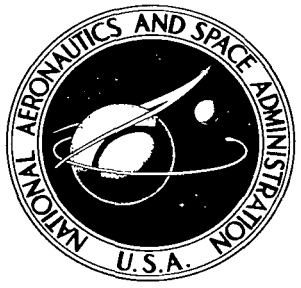

NASA TN D-3797

LARGE-SCALE WIND-TUNNEL TESTS OF A SUBSONIC TRANSPORT WITH AFT ENGINE NACELLES AND HIGH TAIL

by Kiyoshi Aoyagi and William H. Tolhurst, Jr.

Ames Research Center
Moffett Field, Calif.

NATIONAL AERONAUTICS AND SPACE ADMINISTRATION • WASHINGTON, D. C. • JANUARY 1967

NASA TN D-3797

LARGE-SCALE WIND-TUNNEL TESTS OF A SUBSONIC TRANSPORT WITH AFT ENGINE NACELLES AND HIGH TAIL

By Kiyoshi Aoyagi and William H. Tolhurst, Jr.

Ames Research Center
Moffett Field, Calif.

NATIONAL AERONAUTICS AND SPACE ADMINISTRATION

For sale by the Clearinghouse for Federal Scientific and Technical Information
Springfield, Virginia 22151 – Price $2.00

LARGE-SCALE WIND-TUNNEL TESTS OF A SUBSONIC TRANSPORT WITH AFT ENGINE NACELLES AND HIGH TAIL

By Kiyoshi Aoyagi and William H. Tolhurst, Jr.
Ames Research Center

SUMMARY

The static longitudinal stability and control effectiveness at angles of attack above those for wing stall was investigated for a large-scale subsonic transport model with a 35° swept wing of aspect ratio 5.38. The model was tested with the nacelles in several locations and with wing leading- and trailing-edge high lift devices. Pitching moment and longitudinal control characteristics of the model and three-component longitudinal data are presented. Downwash angles and dynamic pressures in the horizontal tail plane location and nacelle inlet pressures are also presented.

The static longitudinal stability and control effectiveness of the model was reduced substantially at angles of attack above that for wing stall. The nacelles did not decrease the longitudinal stability and control effectiveness of the model, compared to that without nacelles, for angles of attack up to 30°. At larger angles the presence of nacelles did reduce the stability of the model. Small changes in the nacelle locations or deflections of the trailing-edge flaps did not significantly improve the longitudinal stability or control effectiveness of the model. However, the use of leading-edge slats with or without trailing-edge flaps did improve both of these characteristics at angles of attack above the wing stalling angle. Sideslipping the model seemed to improve the pitching-moment characteristics.

INTRODUCTION

Flight tests of subsonic transports that have jet engines mounted at the rear of the fuselage and have the horizontal tail on top of the vertical tail indicate that airplanes having this general arrangement may inadvertently pitch up to angles of attack above that for wing stall. Studies (refs. 1 through 3) have shown that the high tail location usually increases the tendency for the pitching-moment variation with angle of attack to be unstable at and above the wing stalling angle. In order to study other factors affecting the post-stall longitudinal stability and control of a configuration with a high tail and aft-mounted nacelles, NASA has undertaken a number of wind-tunnel investigations. References 4, 5, and 6 present the effects of configuration variables on the longitudinal stability and control of a small scale model at Reynolds numbers of 0.8×10^6 to 3.0×10^6.

The present investigation was conducted to determine the post-stall static longitudinal stability and control characteristics of a large-scale research model at high Reynolds numbers and to explore methods of improving these characteristics. Results were obtained with the nacelles in several

locations and with wing leading- and trailing-edge devices. The downwash and flow field at the horizontal tail plane and pressures at the nacelle inlet were measured at angles of attack above the stall angle. All of the data except those for variable Reynolds number were obtained at a Reynolds number of 6.5×10^6, based on a mean aerodynamic chord of 7.96 feet and a dynamic pressure of 20 pounds per square foot.

NOTATION

b	wing span, ft
c	wing chord measured parallel to the plane of symmetry, ft
$\bar{c}$	mean aerodynamic chord, $\frac{2}{S}\int_0^{b/2} c^2\,dy$, ft
C_l	rolling-moment coefficient about stability axis, $\frac{\text{rolling moment}}{q_\infty Sb}$
C_D	drag coefficient, $\frac{\text{drag}}{q_\infty S}$
C_L	lift coefficient, $\frac{\text{lift}}{q_\infty S}$
C_m	pitching-moment coefficient about $0.44\bar{c}$, $\frac{\text{pitching moment}}{q_\infty S\bar{c}}$
C_n	yawing-moment coefficient about stability axis, $\frac{\text{yawing moment}}{q_\infty Sb}$
C_y	side-force coefficient, $\frac{\text{side force}}{q_\infty S}$
i_t	horizontal-tail incidence angle, deg
P_T	total pressure, in. Hg
q	dynamic pressure, lb/sq ft
q_t	dynamic pressure at the horizontal-tail plane, lb/sq ft
R	Reynolds number, $\frac{V_\infty\bar{c}}{\nu}$
S	wing area, sq ft
V_∞	free-stream air velocity, ft/sec
y	spanwise distance perpendicular to the plane of symmetry, ft

α angle of attack of wing, deg

δ_f trailing-edge flap deflections measured normal to the hinge line, deg

δ_S slat deflection measured perpendicular to the leading edge, deg

ϵ downwash angle at the tail location with respect to free stream, deg

η wing semispan station, $\frac{y}{b/2}$

$\Lambda_{c/4}$ sweep angle of quarter chord line, deg

ν free-stream kinematic viscosity, ft^2/sec

Subscripts

t tail

u uncorrected

∞ free stream

MODEL AND APPARATUS

In figure 1 the model is shown mounted in the Ames 40- by 80-foot wind-tunnel. Pertinent dimensions of the basic model configuration are given in figure 2(a).

Wing

The wing had a quarter chord sweep of 35°, an aspect ratio of 5.38, a taper ratio of 0.23, and a dihedral of 3°. The airfoil section was an NACA 65-412 section from the tip to 0.37 of the wing semispan. Inboard of 0.37 semispan, a chord extension added at the trailing edge changed the trailing-edge sweep from 23° to 0° (see fig. 2(b)).

High Lift Devices

Conventional leading-edge slats and trailing-edge flaps were provided for the wing as shown in figures 2(c) and (d), respectively. The slats extended either the full span or half the span of the wing with a δ_S of 20°. Single slotted flaps extended from 0.11 to 0.53 of the wing semispan and were deflected 40°.

Fuselage

The fuselage had a constant 4-foot diameter except at the nose and tail. Both of these sections had elliptical outlines with circular cross sections that decreased from 4 feet to a smaller diameter.

Nacelles

Nacelle details and locations are shown in figure 2(e). The nacelles could be located at the rear of the fuselage at three longitudinal and two spanwise positions. The longitudinal positions were varied by moving the nacelle and pylon together fore and aft on rails; the extreme positions were physically limited because of structural interference. The spanwise positions were varied by moving the nacelle support strut normal to the model centerline.

Tail

The geometry of the horizontal and vertical tails is described in figure 2(a). Pitch control was provided by an all-movable tail that was variable from -20° to $+20^{\circ}$ and by a 25-percent-chord elevator that was also variable -20° to $+20^{\circ}$. The vertical tail was fixed.

Instrumentation

Forces and moments were measured on the wind-tunnel six-component balance.

Dynamic pressure and flow direction were measured at the pivot axis of horizontal-tail plane by directional pitot-static probes at four spanwise stations.

Nacelle inlet flow distortions were measured with four total pressure rakes located close to the inlet lip and spaced 90° apart around the circumference. Each rake contained four pressure probes located at the center of equal areas.

TESTING AND PROCEDURE

Forces and moments were measured for the model through an angle-of-attack range from 0° to 40°. Pitching-moment data were computed about a moment center located at $0.44\bar{c}$. This center was chosen to represent the static margin of a typical high-tailed, rear-engined transport with an aft center of gravity location. All tests except those to show Reynolds number effect were conducted at a Reynolds number of 6.5×10^6, based on a mean aerodynamic chord of 7.96 feet and a dynamic pressure of 20 pounds per square foot.

Tests were conducted with the basic configuration at several tail incidences and elevator settings. Similarly, tests were conducted with several nacelle positions (see fig. 2(e)) and with the nacelles removed. Tail incidence ranged from -10° to $+21^{\circ}$, and the elevators were set at 0° and 20°. Sideslip angle ranged from 0° to -9°, and Reynolds number was varied from 3.8×10^{6} to 8.0×10^{6}, based on a mean aerodynamic chord of 7.96 feet and dynamic pressure range of 5 to 30 pounds per square foot. Maximum angle of attack at a Reynolds number of 8.0×10^{6} was 20° because of a model load limitation.

CORRECTIONS

All data were corrected for strut tares and wind-tunnel-wall effects. Drag and pitching-moment tares due to the support struts were based on data obtained with the struts alone. Corrections for wind-tunnel-wall effect were as follows:

$$\Delta\alpha = 0.527\ C_L$$

$$\Delta C_D = 0.0092\ C_L$$

$$\Delta C_m = 0.0144\ C_L \text{ (tail on tests only)}$$

RESULTS

Table I is an index to the configurations and variables tested and the figures in which the results are presented. Figures 3 through 10 show the variation of pitching-moment coefficient with angle of attack; figures 11 through 18 show three-component longitudinal force and moment data. Figures 19 through 23 present lateral characteristics and show downwash and dynamic pressure data at the tail location and total pressure distortion at the nacelle inlet.

DISCUSSION

Longitudinal Characteristics

Basic configuration characteristics.- Figure 3 shows that for less than 10° tail incidence the model was statically stable to an angle of attack of about 16°. Tuft studies and the reduction in lift coefficient (fig. 11) indicated that the wing stalled at about 16°. From 16° to 20° angle of attack the model was unstable with the tail off or on. The progression of air-flow separation from the tip of the wing inboard and the increase of downwash angle with angle of attack (fig. 21) caused the instability. From an angle of attack of about 20° to 24° the model was statically stable for tail incidences above 15° because the large downwash angle unstalled the tail.

At angles of attack above 24° static margin was largely a function of the tail moment contribution since the tail-off configuration was neutrally stable (fig. 3(a)). This contribution decreased substantially above 24° angle of attack due to a reduction of dynamic pressure at the tail (shown in fig. 21).

Tail effectiveness and elevator control power were reduced substantially at angles of attack above that for wing stall (see fig. 3). For example, at an angle of attack of 30°, the effectiveness was approximately half that at an angle of attack of 16° (when the tail was unstalled) because of the large reduction in dynamic pressure at the tail. For tail incidences of 10° or more, the tail stalled at angles of attack below that for wing stall. Consequently, control effectiveness was less than that at lower tail incidences. At angles of attack above that for wing stall the large downwash angle unstalled the tail; thus, longitudinal control power increased at angles of attack above 24° for tail incidences of 15° and 20°. This could be used as a possible means of recovery from extremely high angles of attack.

The results presented are for the center of gravity at $0.44\bar{c}$ which gave a static margin of 27.5 percent at angles of attack below that for wing stall. An aircraft with a less stable static margin could be unstable at all angles of attack above that for wing stall.

Effect of nacelle and location.- The effect of nacelles on the variation of pitching moment and longitudinal control characteristics of the model with angle of attack (fig. 4) was small up to an angle of attack of approximately 30°. At larger angles the nacelles reduced the stability; limited downwash data above 30° angle of attack (fig. 21) indicate that the nacelles increased downwash angles at the tail. The variation of nacelle spanwise and longitudinal positions (figs. 4 and 5), within the range tested, had little effect on the pitching-moment characteristics of the model. Results obtained for a larger range of longitudinal positions, $0.93\bar{c}$ forward and $0.60\bar{c}$ aft (ref. 6), show an effect of nacelle location.

Effect of high-lift devices.- The effect of high-lift devices on the pitching-moment and longitudinal control characteristics was explored. Configurations tested included leading-edge slats alone and trailing-edge flaps with and without slats. The data in figures 6 and 7 are for the half-span leading-edge slats located on either the inboard or the outboard portion of the wing. In comparing these data, it should be noted that they are for different nacelle positions. Neither slat location eliminated the instability at wing stall, but the outboard slats did increase the angle of attack for wing stall (see fig. 15). The inboard slats increased the longitudinal control power at angles of attack above the wing stalling angle, but the outboard slats did not.

The effect of trailing-edge flaps, both with and without slats, on the pitching-moment variation with angle of attack is shown in figure 8. With the flaps deflected and the slats off, this variation was similar to that of the basic configuration. When the flaps were combined with the full-span leading-edge slats, the pitching-moment variation was neutrally stable from an angle of attack of 13° to 20°. At larger angles of attack the pitching-moment variation with the half-span and the full-span slats was similar.

Pitching and Rolling Moments With Sideslip Angle

The effect of sideslip angle on the variation of pitching and rolling moments with angle of attack is shown in figures 9 and 19. Sideslip angle increased rolling moments and reduced pitching-moment variation in the angle-of-attack range above that for wing stall. When longitudinal control is limited, both these characteristics could be advantageous in recovery from deep stall, but further investigation of lateral and directional controls at angles of attack above the wing stalling angle are required.

Total Pressure Distortions at the Nacelle Inlet

Total pressure distortion was very small until the angle of attack was above that for wing stall. For the nacelle positions tested, the maximum distortion ($P_{T_{max}} - P_{T_{min}} / P_{T_{av}}$) was 0.3 of 1 percent which is well within the usual allowable distortion limits of current jet engines. The operation of engines at angles of attack above the wing stalling angle is therefore probably feasible.

CONCLUDING REMARKS

In general, the pitching-moment characteristics of the model above the angles of attack for wing stall resulted in a substantial reduction in stability and longitudinal control effectiveness. The presence of nacelles and pylons mounted aft on the fuselage aggravated the instability of the model at angles of attack above that for wing stall. Small changes in the nacelle position (either in the spanwise or longitudinal direction) or deflection of the trailing-edge flaps did not significantly improve the longitudinal stability or increase longitudinal control effectiveness.

The use of leading-edge slats with or without flaps improved both stability and horizontal-tail control effectiveness at angles of attack above the wing stalling angle. Sideslipping the model improved the pitching-moment characteristics.

Ames Research Center
National Aeronautics and Space Administration
Moffett Field, Calif., Oct. 10, 1966
126-13-01-18

REFERENCES

1. Kelly, Mark W.; Tolhurst, William H., Jr.; and Maki, Ralph L.: Full-Scale Wind-Tunnel Tests of a Low-Aspect-Ratio, Straight-Wing Airplane With Blowing Boundary-Layer Control on Leading- and Trailing-Edge Flaps. NASA TN D-135, 1959.

2. Evans, William T.: Data From Flow-Field Surveys Behind a Large-Scale Thin Straight Wing of Aspect Ratio 3. NACA RM A58D17, 1958.

3. Salmi, Reino J.: Horizontal-Tail Effectiveness and Downwash Surveys for Two 47.7° Sweptback Wing-Fuselage Combinations With Aspect Ratios of 5.1 and 6.0 at a Reynolds Number of 6.0×10^6. NACA RM L50K06, 1951.

4. Taylor, Robert; and Ray, Edward J.: A Systematic Study of the Factors Contributing to Post-Stall Longitudinal Stability of T-Tail Transport Configurations. AIAA Paper 65-737.

5. Taylor, Robert; and Ray Edward J.: Factors Affecting the Stability of T-Tail Transports. J. Aircraft, vol. 3, no. 4, July-August 1966, pp. 359-364.

6. Ray, Edward J.; and Taylor, Robert T.: Effect of Configuration Variables on the Subsonic Longitudinal Stability Characteristics of a High-Tail Transport Configuration. NASA TM X-1165, 1965.

TABLE I.- LIST OF FIGURES

Figure	Nacelle position (see fig. 2(e))	δ_f, deg	Span of leading-edge slats	α_u, deg	i_t, deg	δ_e, deg	β, deg	Remarks
Pitching moment and longitudinal control characteristics with variable angle of attack								
3(a)	2	0	None	0 to 40	-10,-5,0,5,10,21 Tail off	0	0	Basic configuration
3(b)					-5,5,10,15,20	20		
4	2,3 Off				-5,10	0,20		Nacelle spanwise positions and removal
5	1,2,4							Nacelle longitudinal positions
6	2		Half-span inboard None		-5			Inboard slats
7	4		Half-span outboard None		-5,10	0,20		Outboard slats
8	2	0	None		-5	0		Flaps alone and combination of slats and flaps
		40	None					
			Full span					
			Half-span outboard			20		
			Full span		10	20		
			Full span					
9	2	0	None		-5	0	0	Sideslip angle
							-3	
							-6,-9	
10(a)	2	0	None		-5	0	0	R = 3.2, 4.6, 6.5, 8.0x10^6
10(b)					Tail off			
10(c)	Off							α_u limited to 20° at R = 8.0x10^6
Longitudinal characteristics of the model								
11(a)	2		None	0 to 40	0,-5,-10,5,10,21 Tail off	0	0	Basic configuration
11(b)					-5,5,10,15,20	20		
12(a)	2,3, Off				-5	0		Nacelle spanwise positions
12(b)	2,3, Off				-5	20		
12(c)	2,3, Off				10	20		
13(a)	1,2,4				-5	20		Nacelle longitudinal positions
13(b)	1,2,4				10	20		
14	2		None Half-span inboard		-5	0,20		Inboard slats
15	4		None Half-span outboard		-5,10	0,20		Outboard slats
16	2	0	None		-5	0		Flaps alone and combination of slats and flaps
		40	None					
			Half-span outboard					
			Full span			20		
			Full span		10	20		
			Full span					
17	2	0	None		-5	0	0	Sideslip angle
							-3	
							-6	
							-9	
18(a)							0	R = 3.2, 4.6, 6.5, 8.0x10^6
18(b)					Tail off			α_u limited to 20° at R = 8.0x10^6
18(c)	Off							
Lateral characteristics of the model with sideslip angle								
19	2	0	None	0 to 40	-5	0	0,-3, -6,-9	Variation with angle of attack
20							0,-3, -6,-9	Variation with lift coefficient
Downwash and dynamic pressure at the tail location								
21(a)	2, Off	0	None	0 to 40	Tail off		0	Nacelle effect
21(b)	2, Off	40	Full span					
Nacelle inlet total pressure distortion								
22(a)	1	0	None	20 to 40	-5	0	0	Nacelle longitudinal position effect
22(b)	2							
22(c)	4			18 to 40	10	20		
23(a)	2	40	None	20 to 40	-5	0		Slat effect
23(b)			Full span	24 to 40				

A-33825

Figure 1.- Photograph of the model mounted in the Ames 40- by 80-foot wind tunnel.

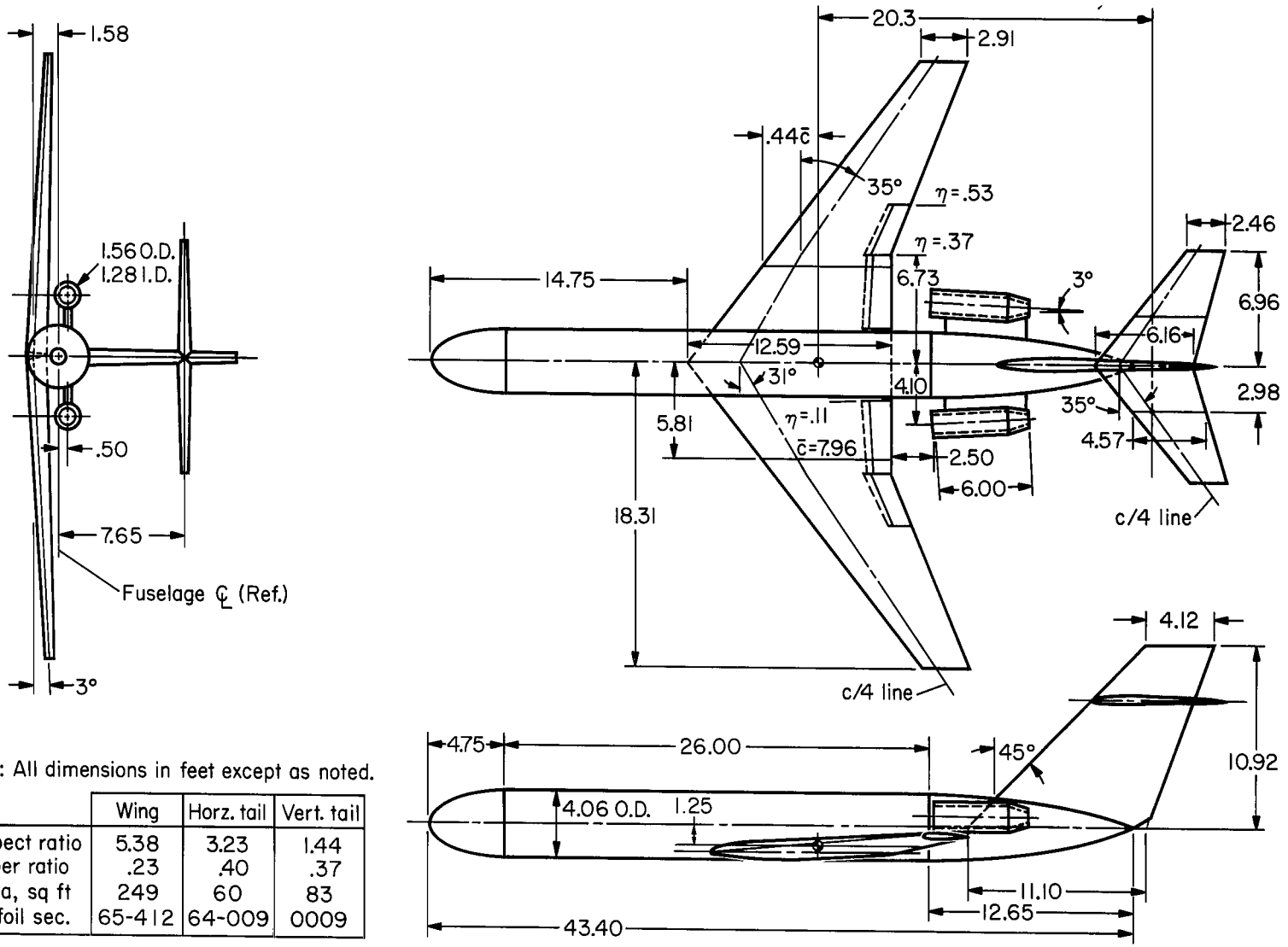

Note: All dimensions in feet except as noted.

	Wing	Horz. tail	Vert. tail
Aspect ratio	5.38	3.23	1.44
Taper ratio	.23	.40	.37
Area, sq ft	249	60	83
Airfoil sec.	65-412	64-009	0009

(a) Basic configuration.

Figure 2.- Geometric details of the model.

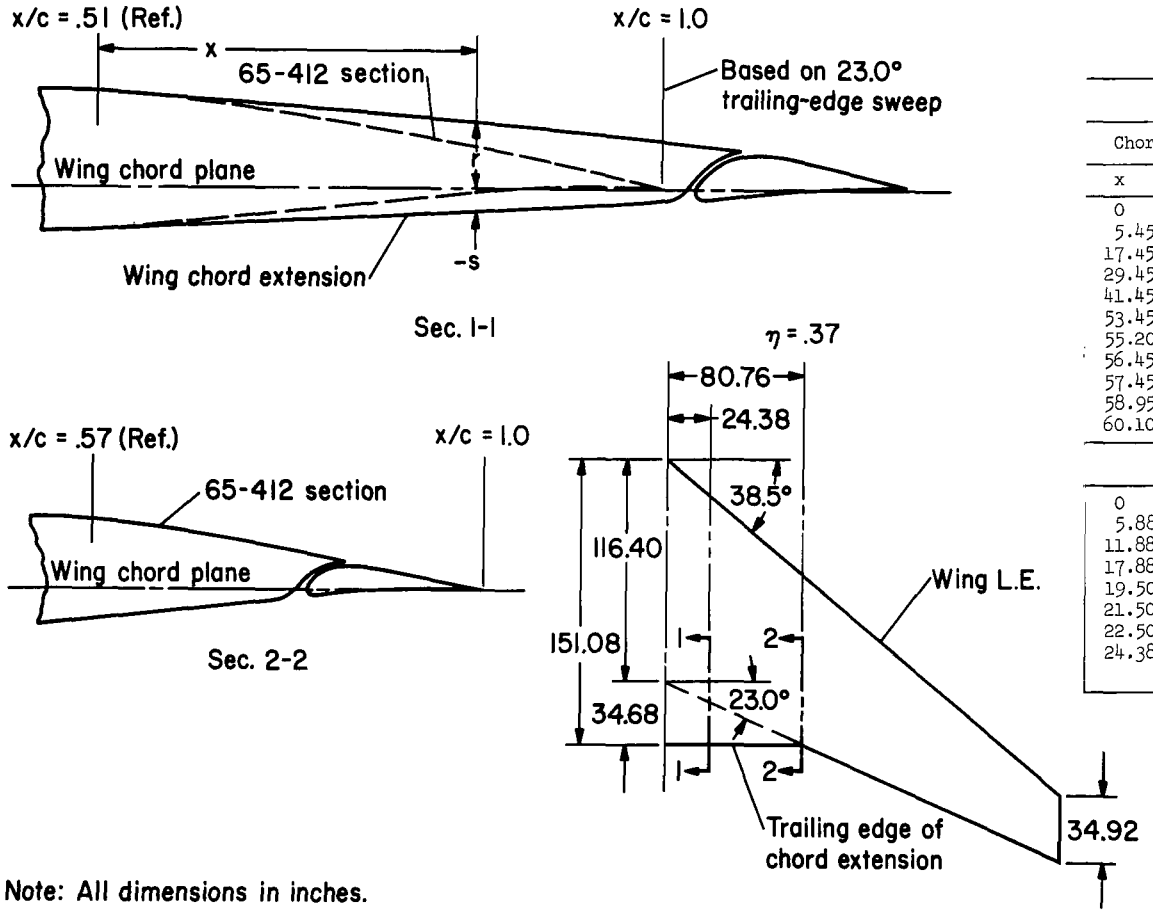

Sec. 1 - 1					
Chord extension			Flap		
x	r	s	x	r	s
0	8.50	-3.80	55.45	-0.43	-0.43
5.45	8.15	-3.53	56.15	1.03	-.93
17.45	7.30	-2.95	57.45	2.23	-.76
29.45	6.40	-2.32	58.45	3.14	---
41.45	5.52	-1.75	60.65	3.30	---
53.45	4.40	-1.06	62.24	3.12	-.29
55.20	4.21	0	66.95	2.09	.10
56.45	4.05	1.55	71.75	1.05	.28
57.45	3.90	2.35	76.60	0	0
58.95	3.70	3.10			
60.10	3.49	3.42			
Sec. 2 - 2					
0	6.35	-2.65	19.88	-.32	-.32
5.88	5.62	-2.05	20.50	.98	-.75
11.88	4.80	-1.45	21.50	1.82	-.61
17.88	3.75	-.92	22.50	2.40	---
19.50	3.50	-.20	23.50	2.63	---
21.50	3.15	1.95	24.50	2.60	-.30
22.50	2.99	2.51	29.00	1.70	.10
24.38	2.70	2.63	32.75	.89	.20
			36.86	0	0

(b) Inboard wing section.

Figure 2.- Continued.

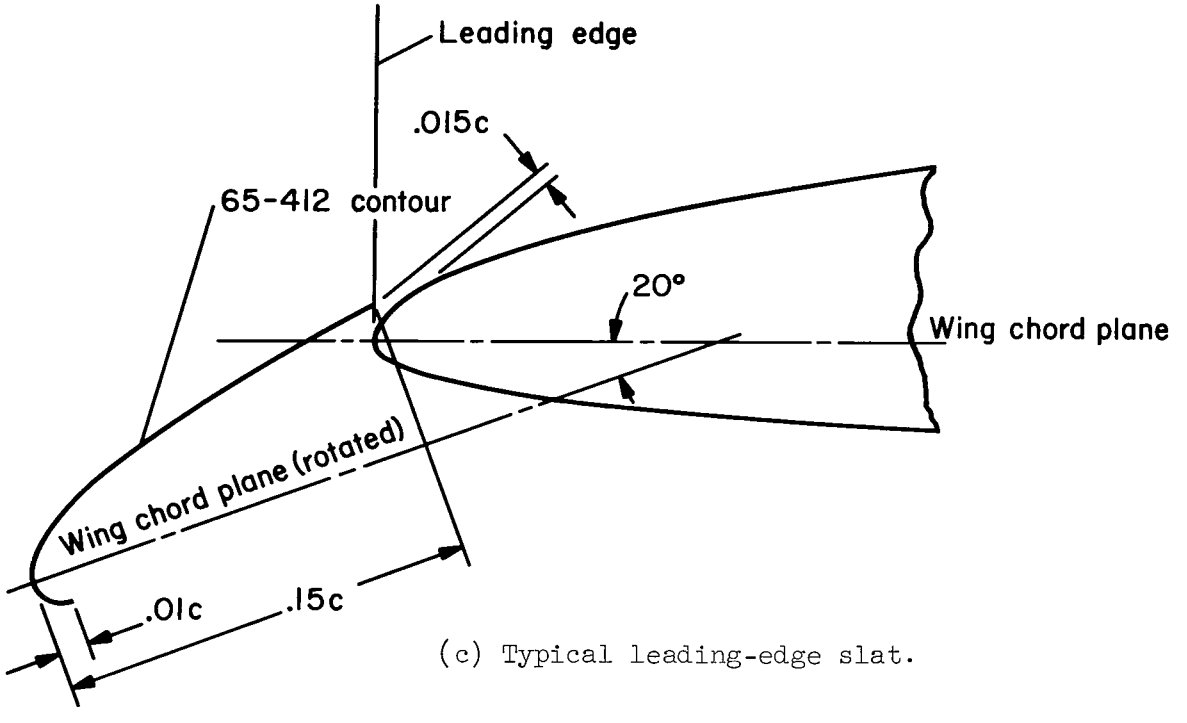

(c) Typical leading-edge slat.

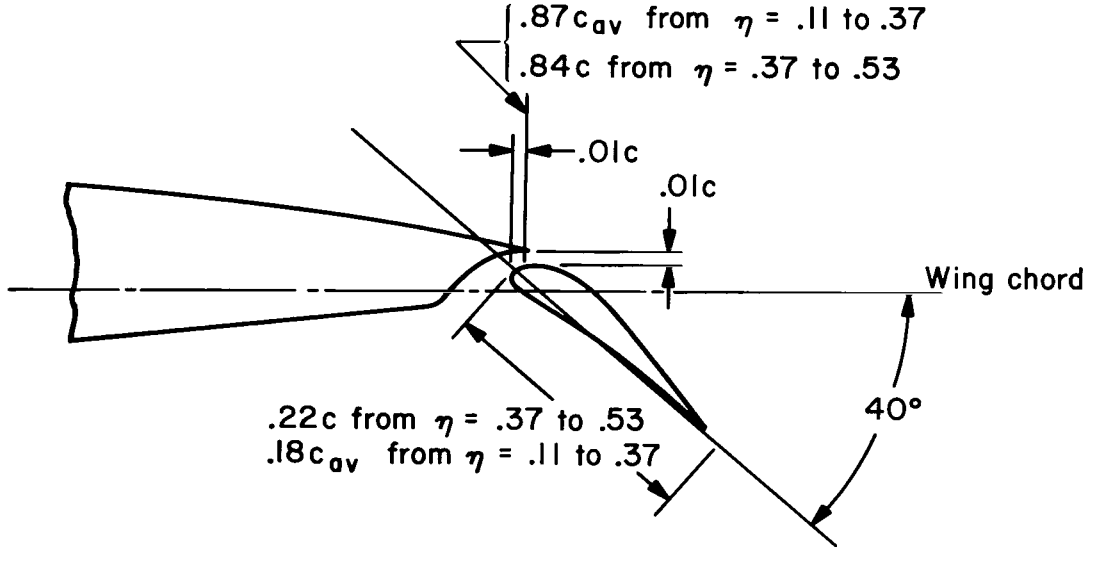

(d) Typical trailing-edge flap.

Figure 2.- Continued.

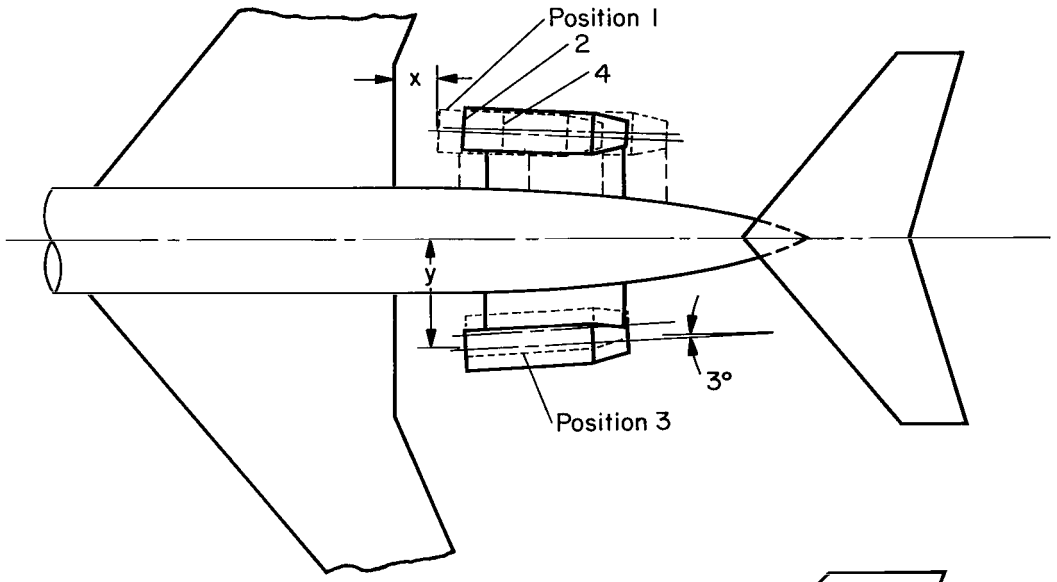

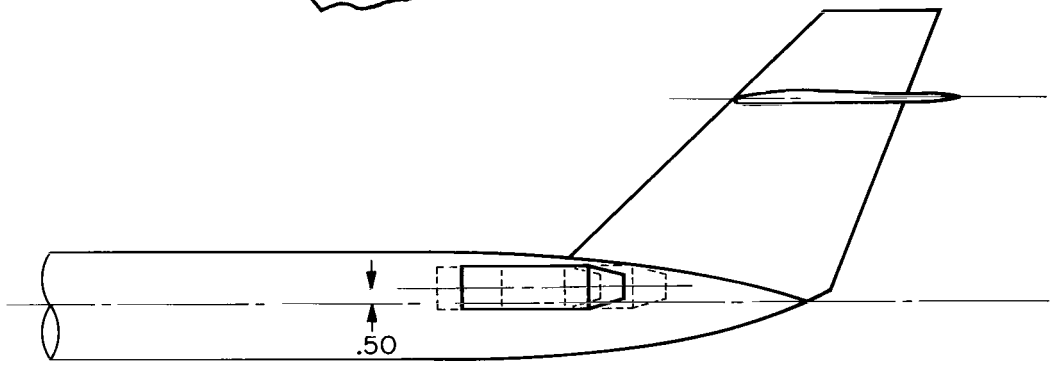

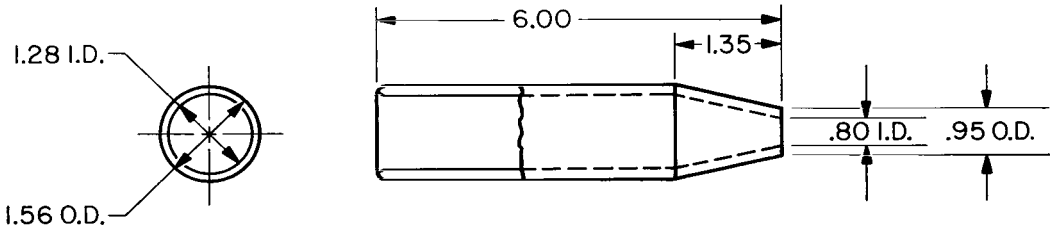

Nacelle positions			
Position	x, ft	y, ft	
		Outboard	Inboard
1	1.6	4.1	—
2	2.5	4.1	—
3	2.5	—	3.5
4	3.8	4.1	—

Note: All dimensions in feet.

(e) Nacelle detail and locations.

Figure 2.- Concluded.

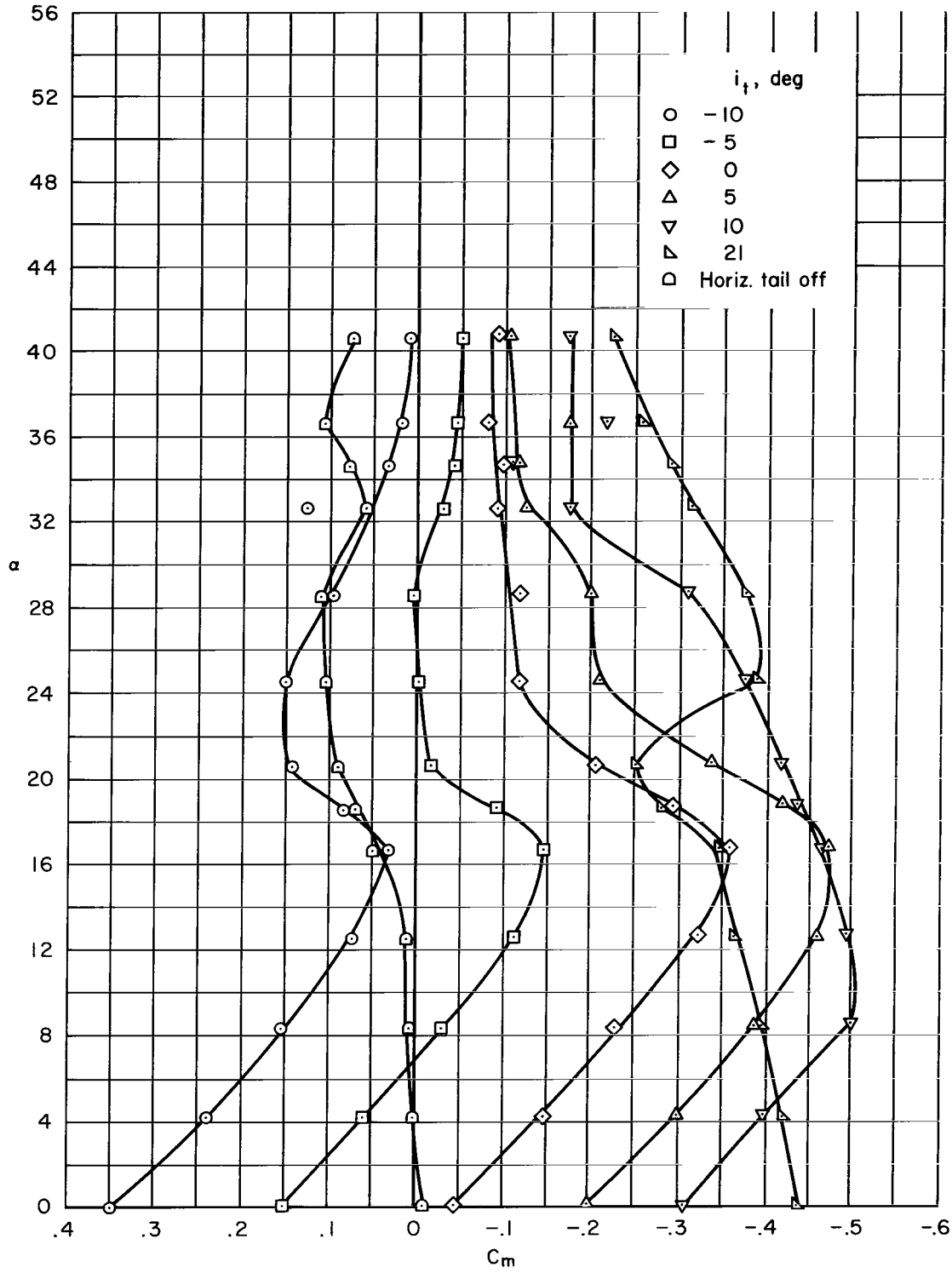

(a) $\delta_e = 0^\circ$

Figure 3.- Effect of horizontal-tail incidence on variation of pitching-moment coefficient with angle of attack; nacelle position 2.

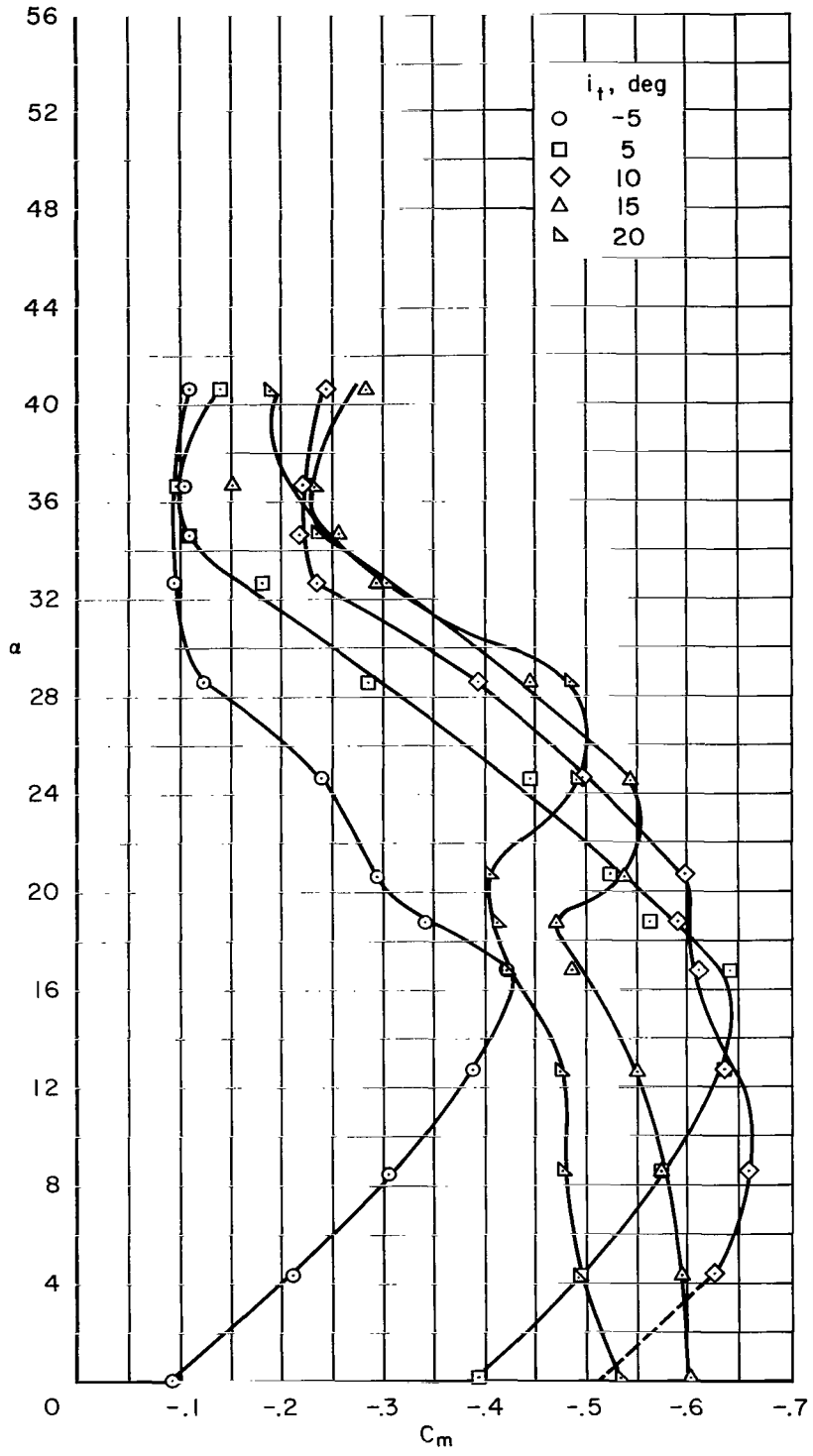

(b) $\delta_e = 20^\circ$

Figure 3.- Concluded.

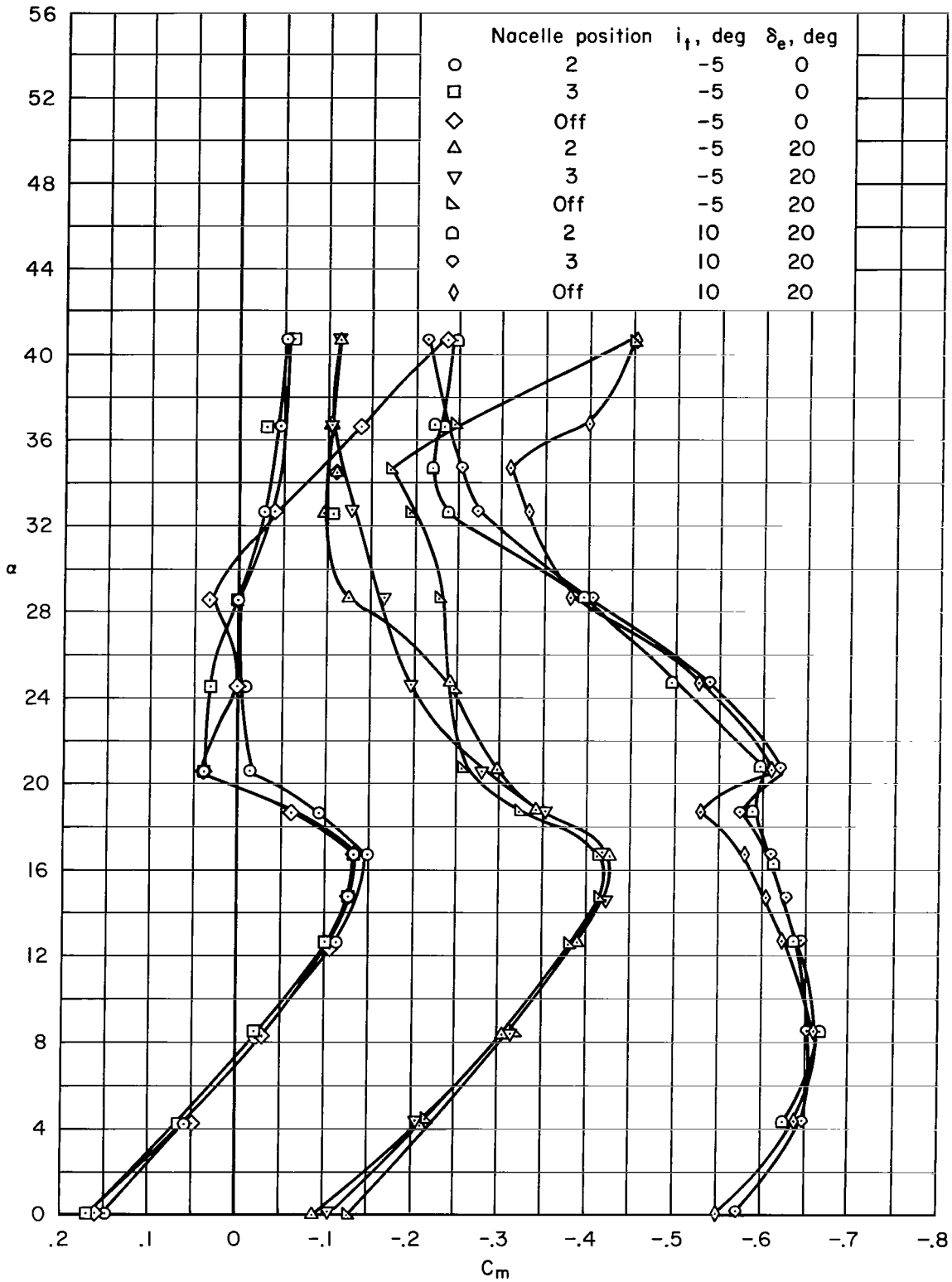

Figure 4.- Effect of nacelle spanwise position on variation of pitching-moment coefficient with angle of attack; $\delta_f = 0^\circ$.

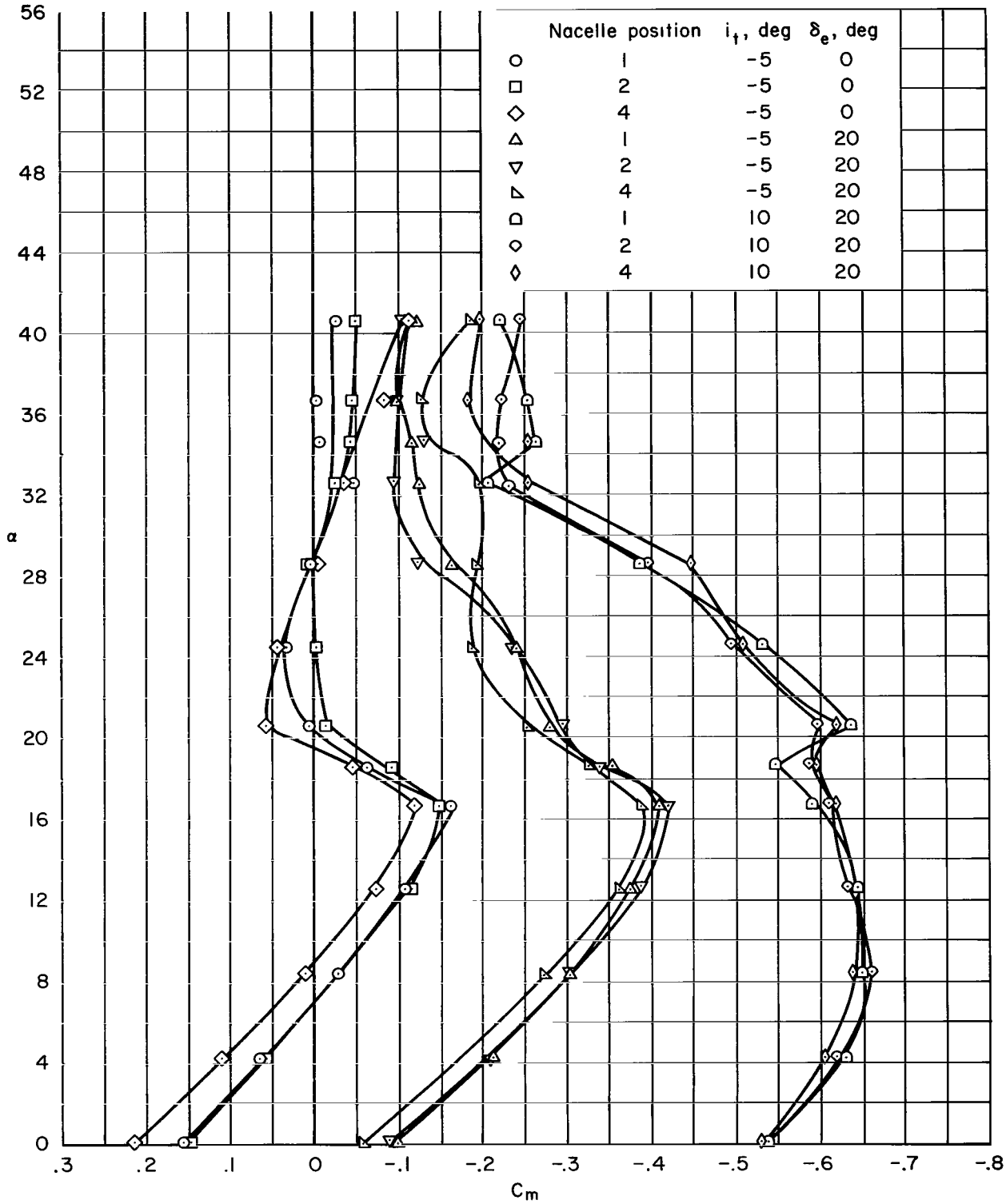

Figure 5.- Effect of nacelle longitudinal position on variation of pitching-moment coefficient with angle of attack; $\delta_f = 0^\circ$.

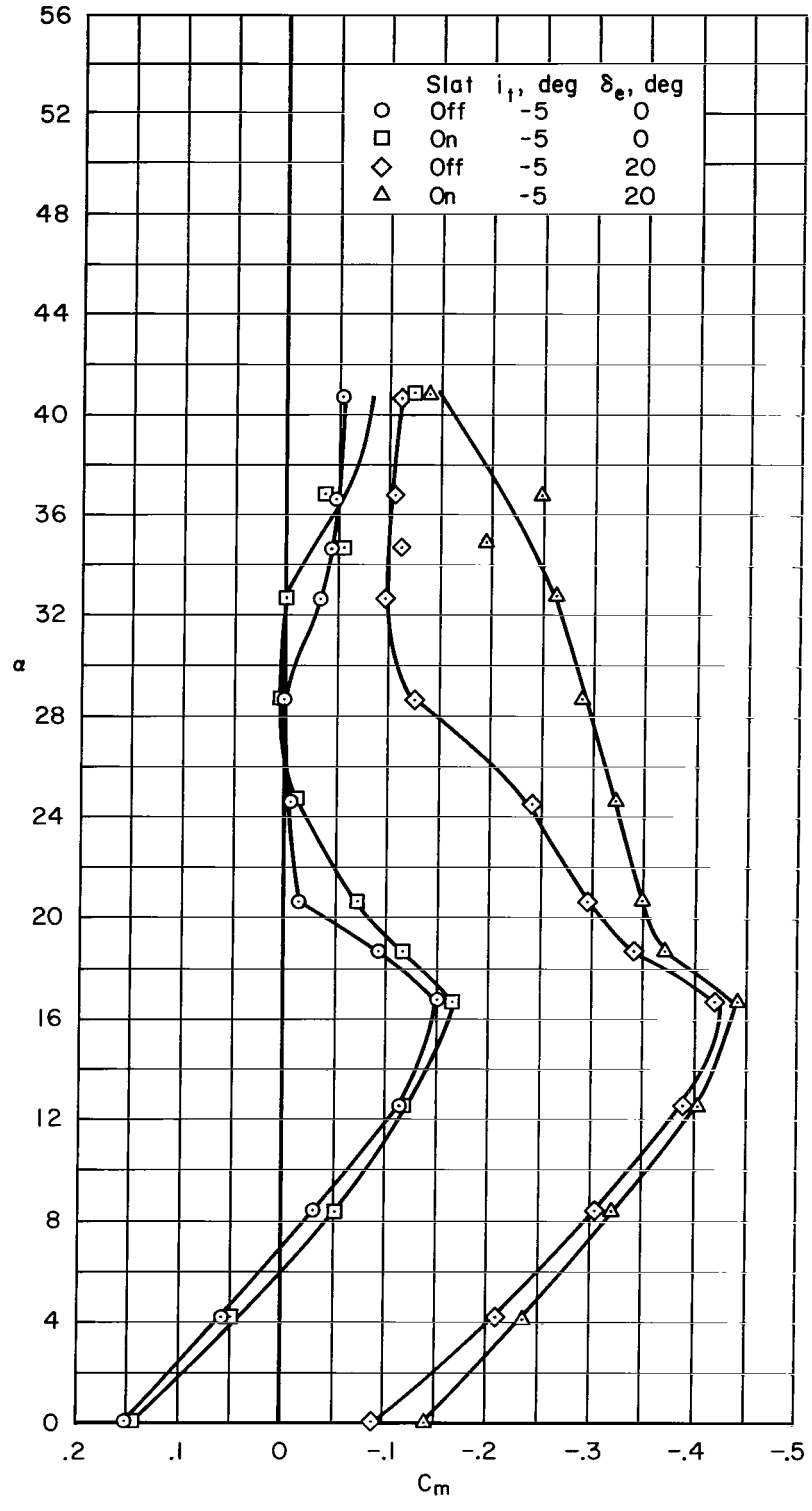

Figure 6.- Effect of half-span inboard leading-edge slats on the variation of pitching-moment coefficient with angle of attack; $\delta_f = 0^\circ$, nacelle position 2.

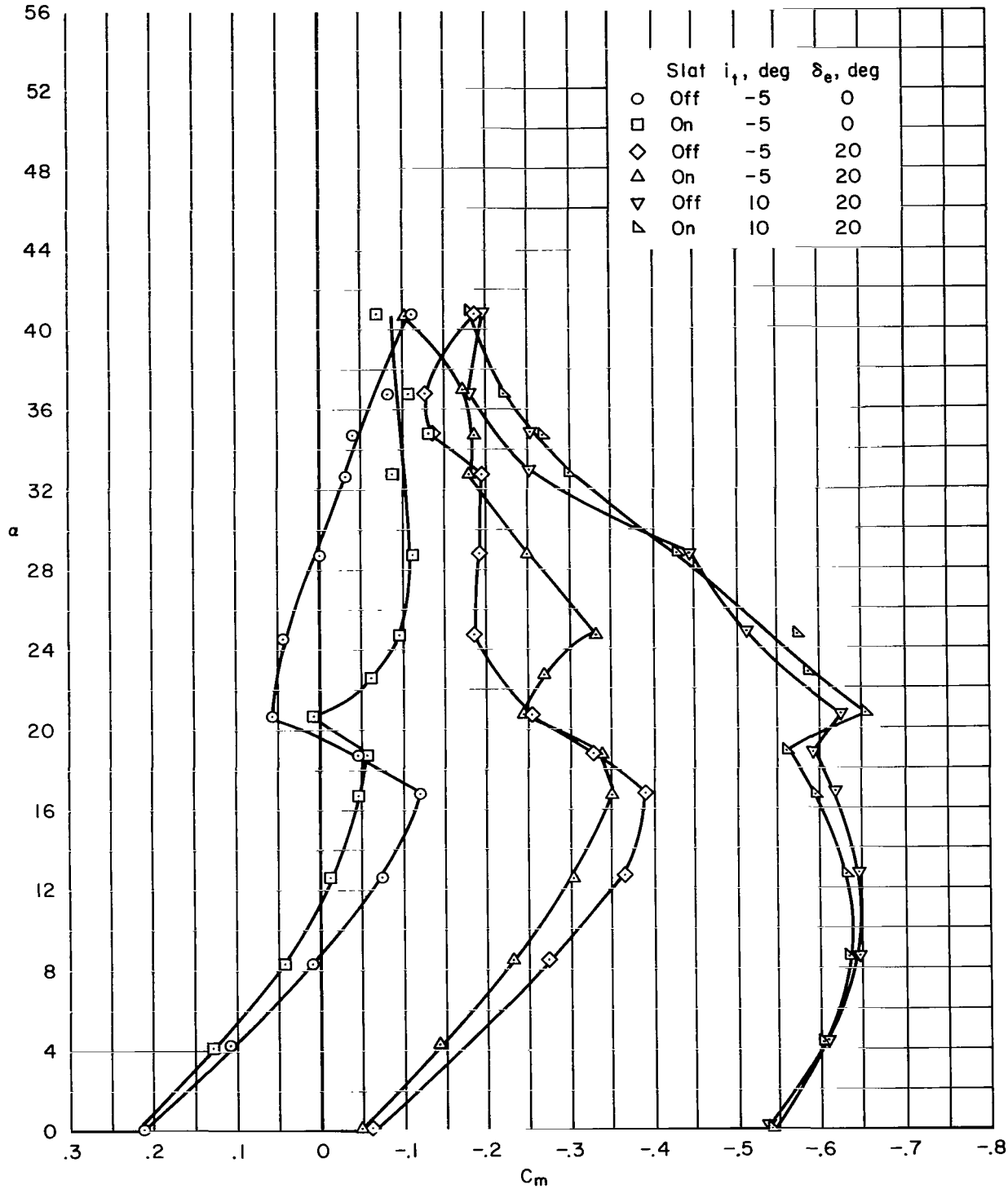

Figure 7.- Effect of half-span outboard leading-edge slats on variation of pitching-moment coefficient with angle of attack; $\delta_f = 0^o$, nacelle position 4.

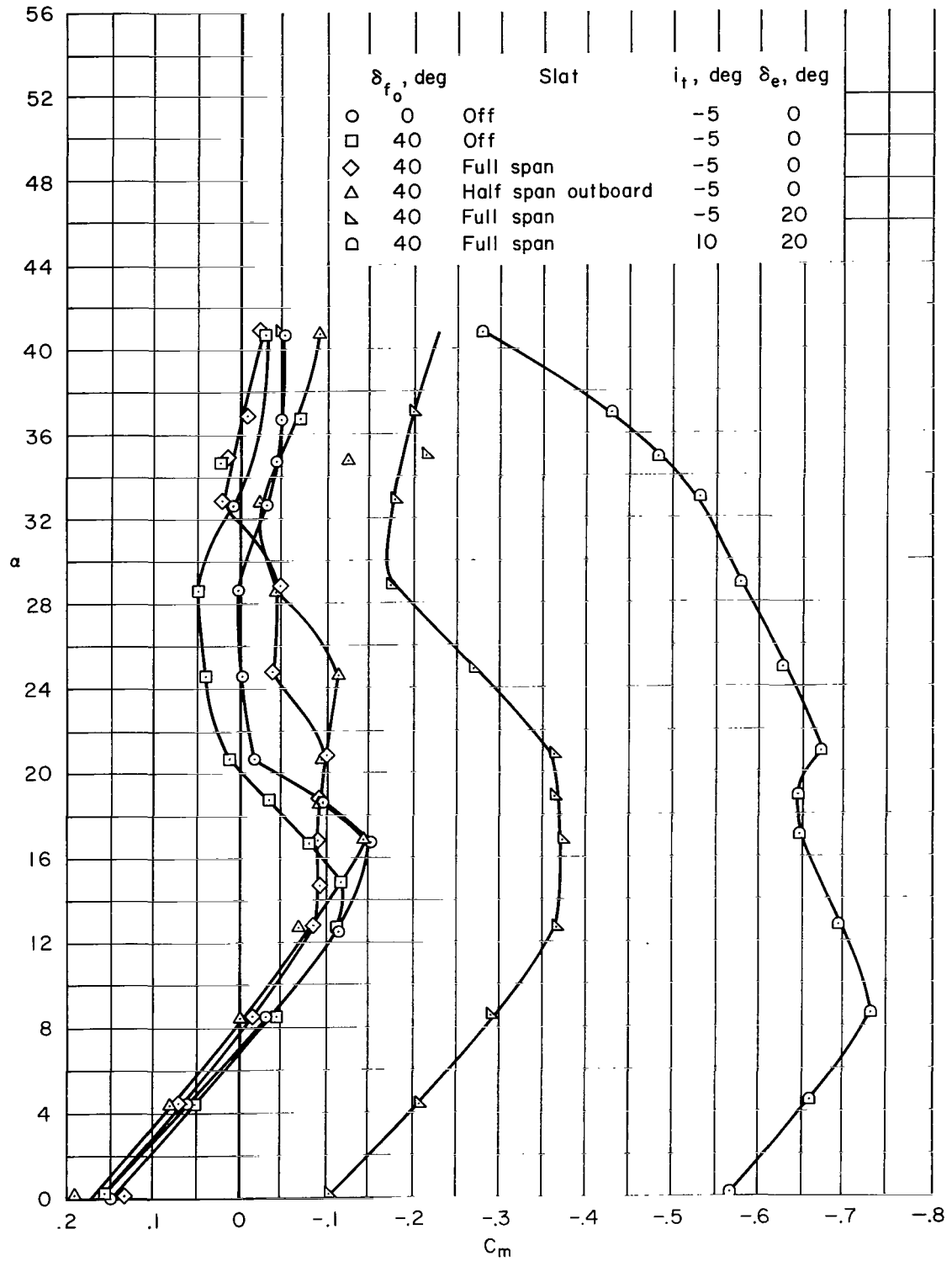

Figure 8.- Effect of leading-edge slats with trailing-edge flap deflected 40° on variation of pitching-moment coefficient with angle of attack; nacelle position 2.

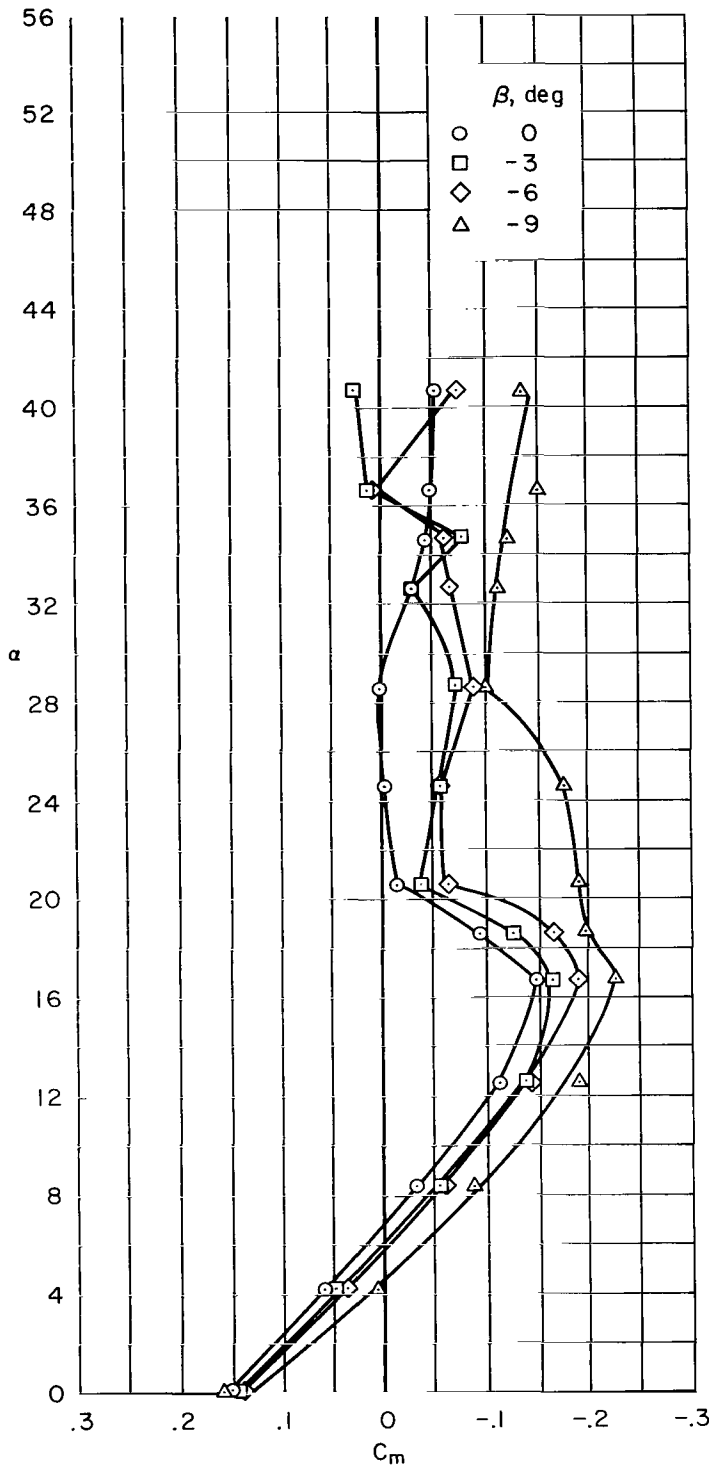

Figure 9.- Effect of sideslip angle on variation of pitching-moment coefficient with angle of attack; $\delta_f = 0^\circ$, nacelle position 2, $i_t = -5^\circ$, $\delta_e = 0^\circ$.

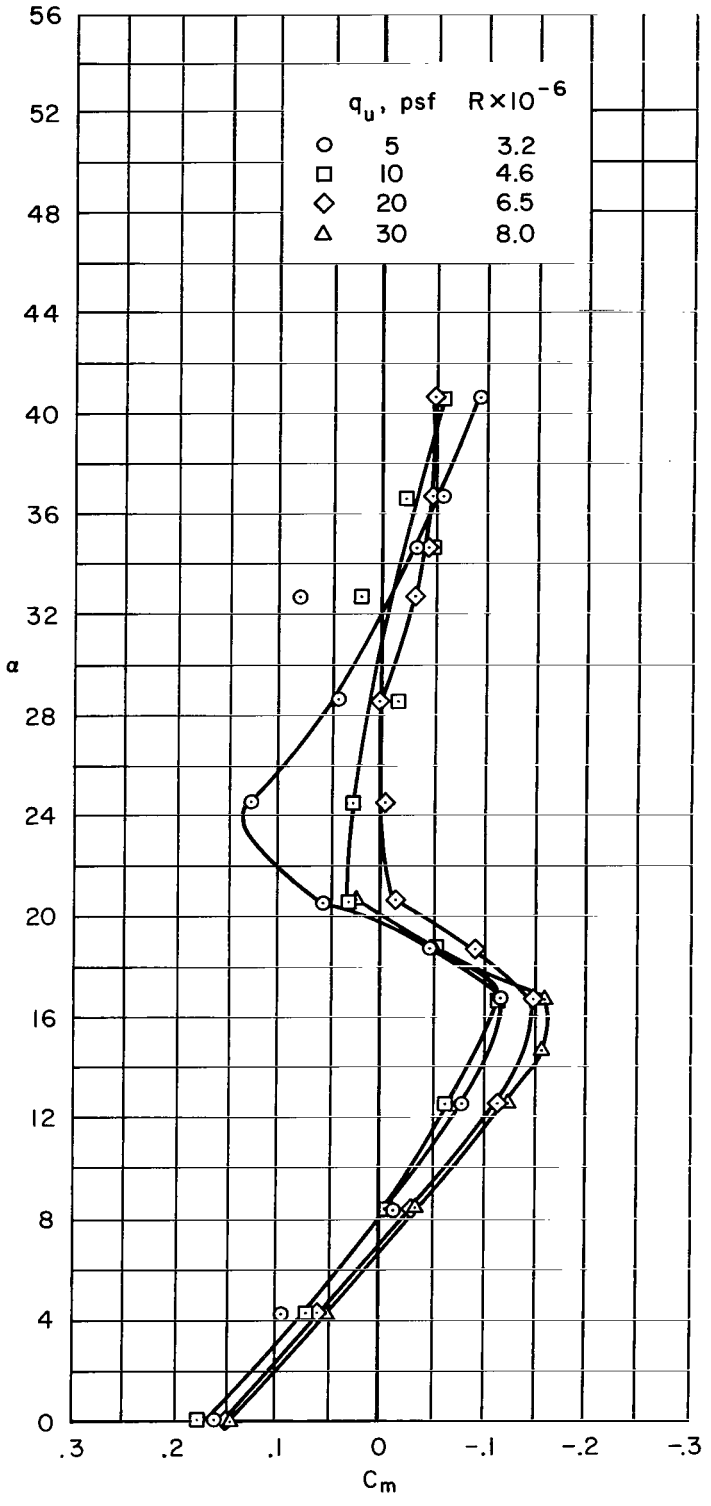

(a) $i_t = -5^\circ$, $\delta_e = 0^\circ$; nacelle position 2.

Figure 10.- Effect of Reynolds number on variation of the pitching-moment coefficient with angle of attack; $\delta_f = 0^\circ$.

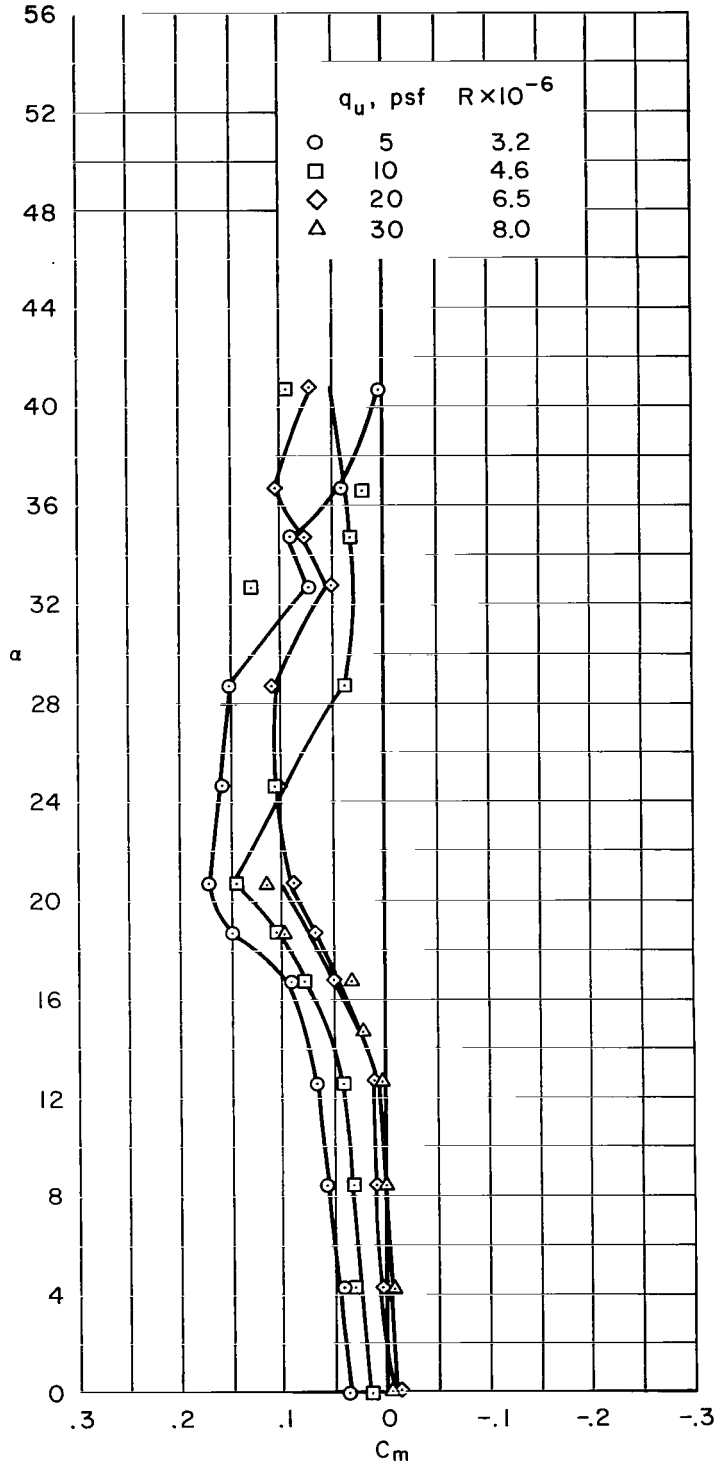

(b) Horizontal tail off; nacelle position 2.

Figure 10.- Continued.

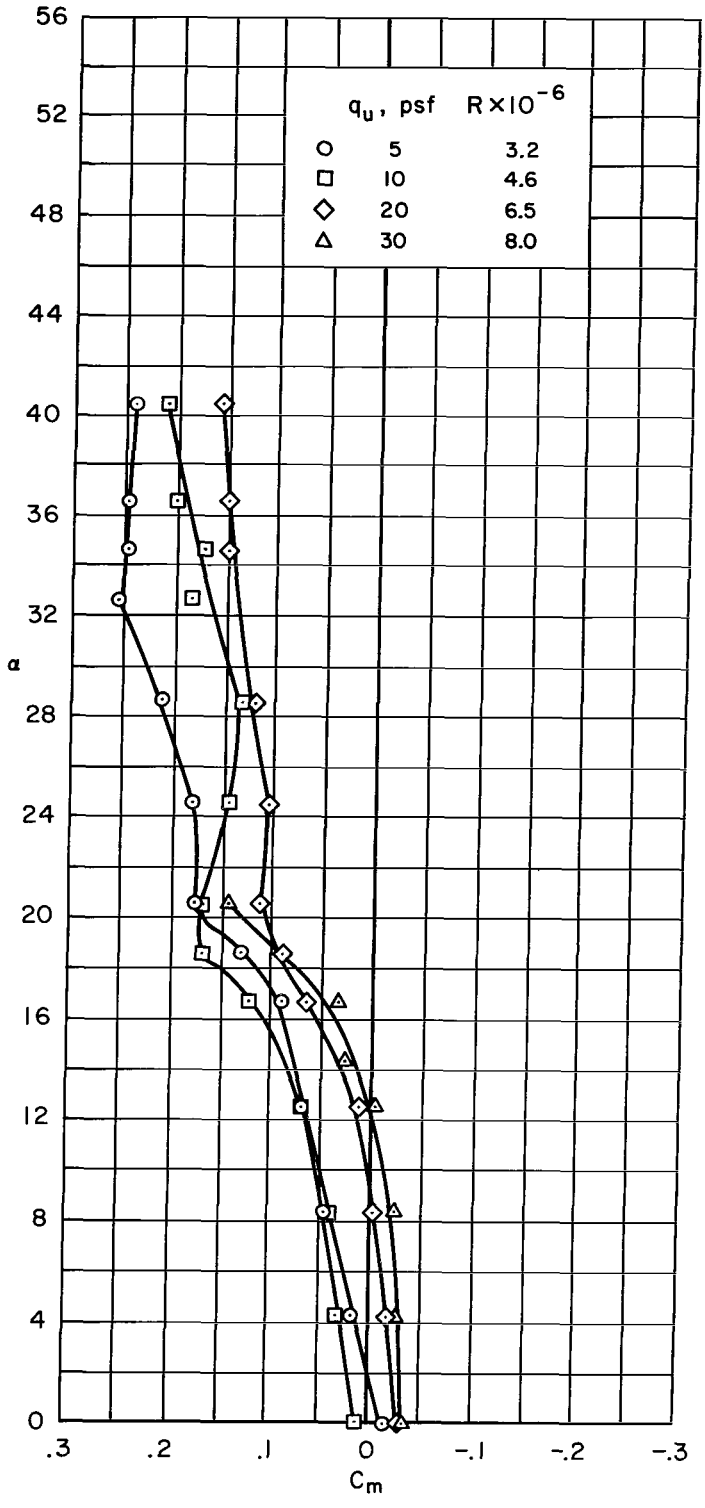

(c) Horizontal tail and nacelles off.

Figure 10.- Concluded.

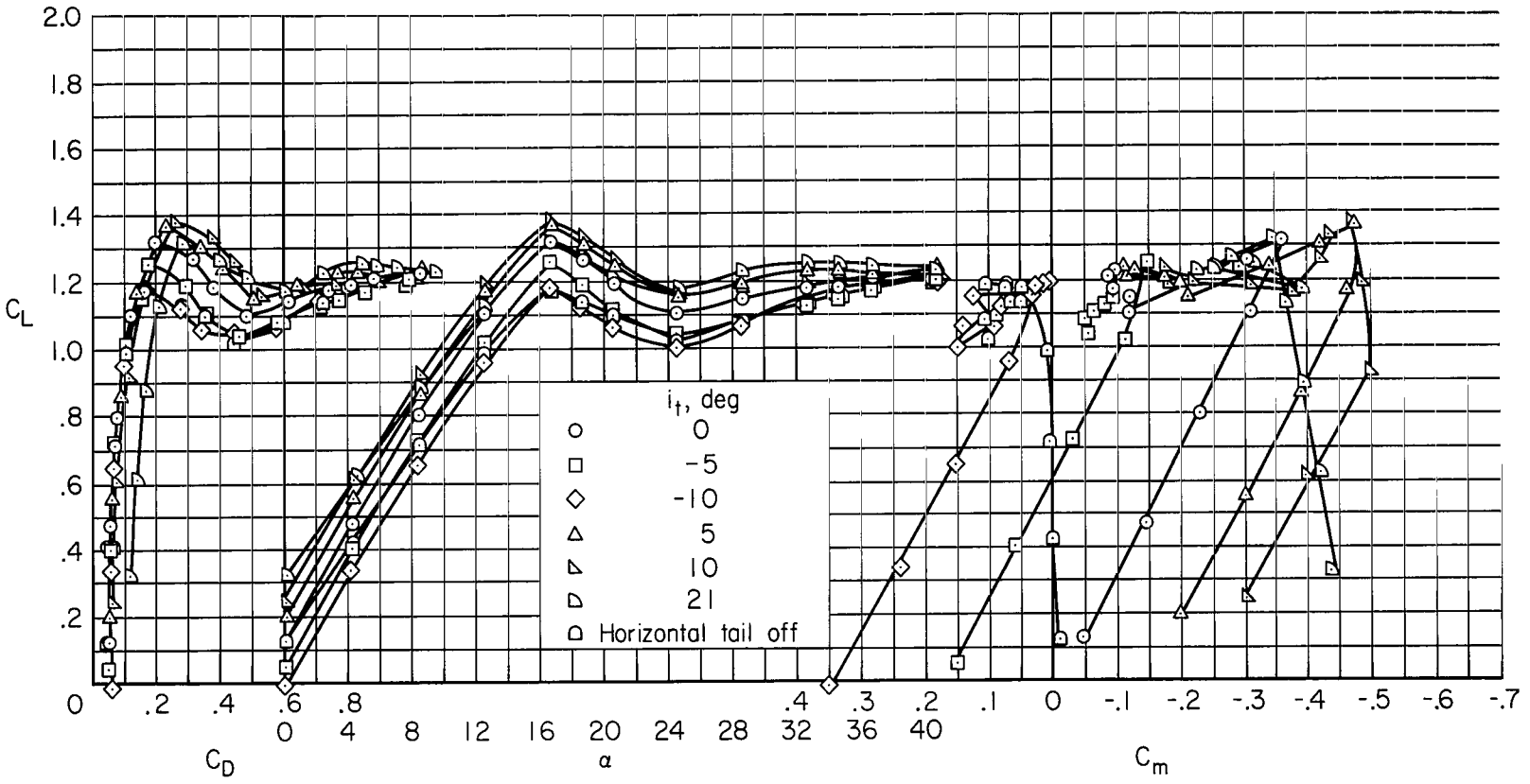

(a) $\delta_e = 0^\circ$

Figure 11.- Effect of horizontal tail incidence on the longitudinal characteristics of the model; $\delta_f = 0^\circ$, nacelle position 2.

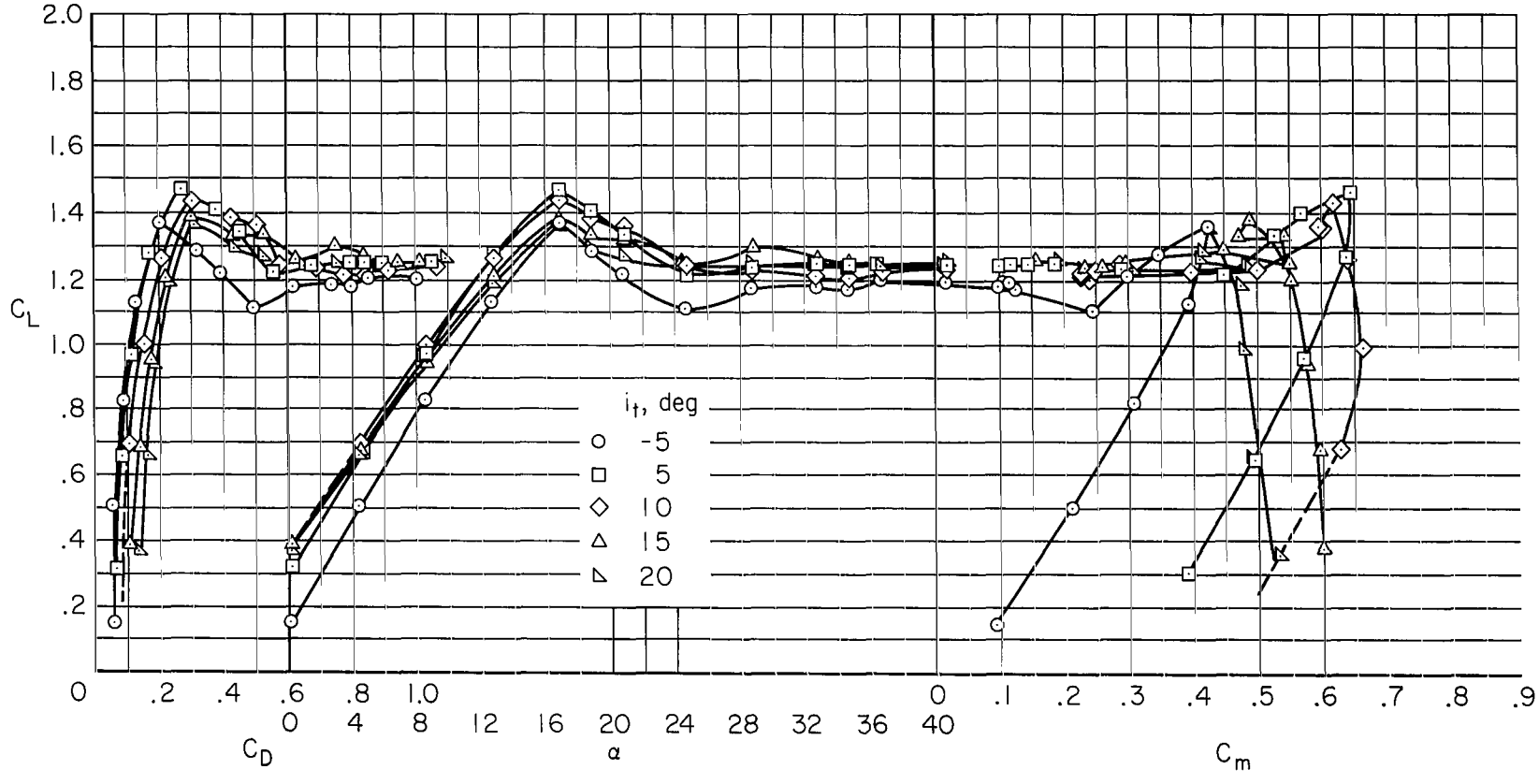

(b) $\delta_e = 20^\circ$

Figure 11.- Concluded.

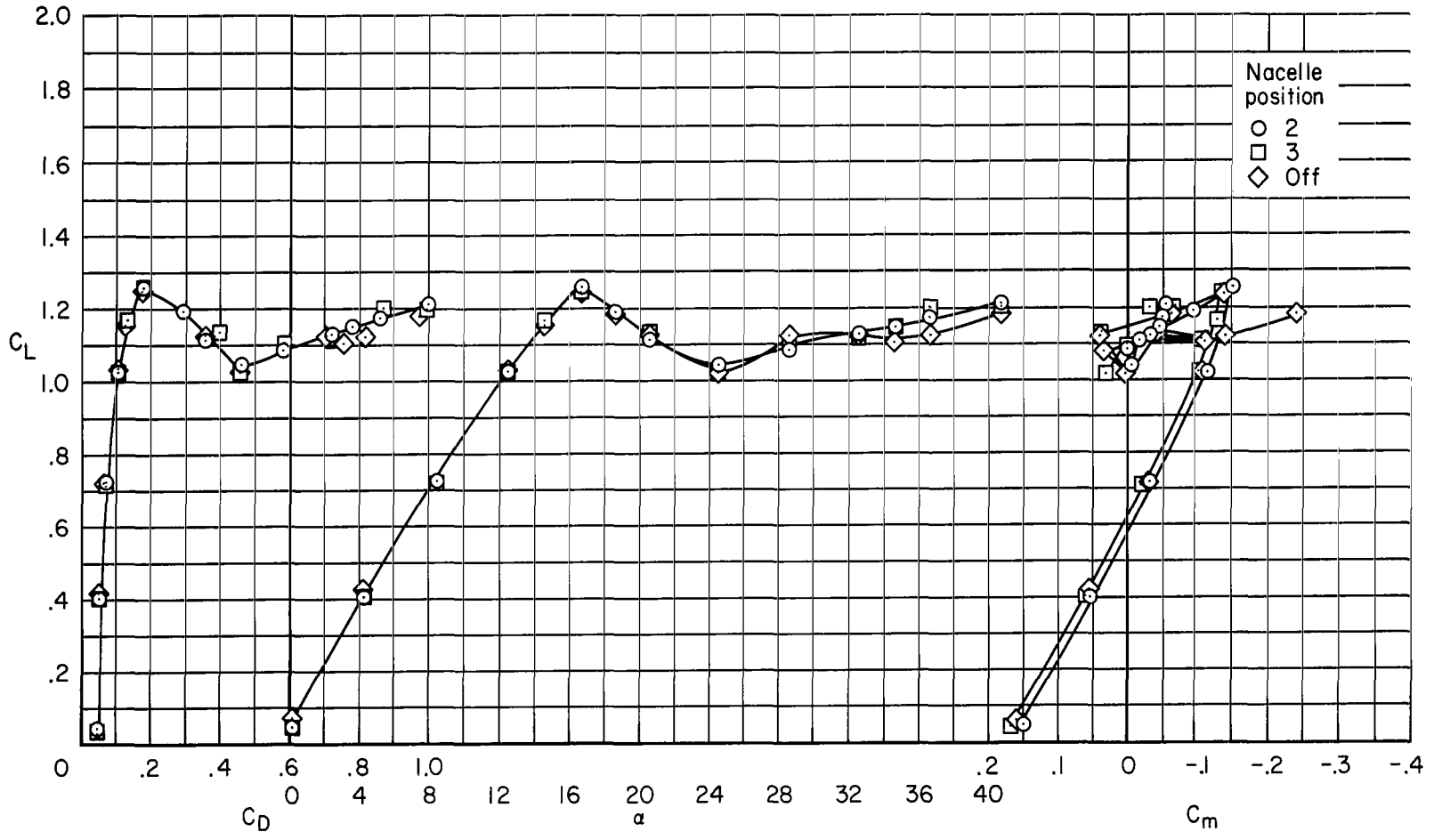

(a) $i_t = -5^\circ$, $\delta_e = 0^\circ$

Figure 12.- Effect of nacelle spanwise extension on the longitudinal characteristics of the model; $\delta_f = 0^\circ$.

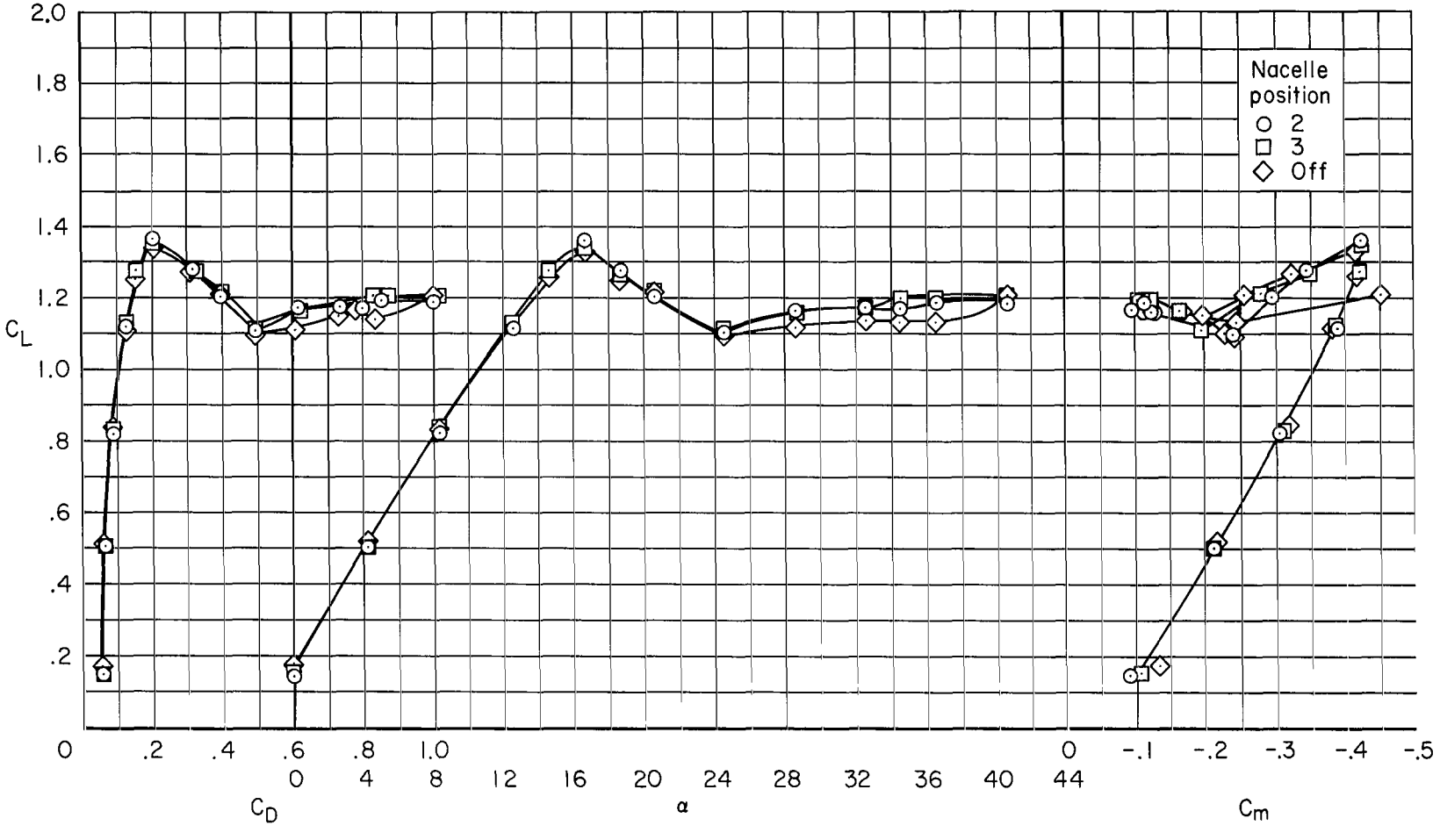

(b) $i_t = -5^\circ$, $\delta_e = 20^\circ$

Figure 12.- Continued.

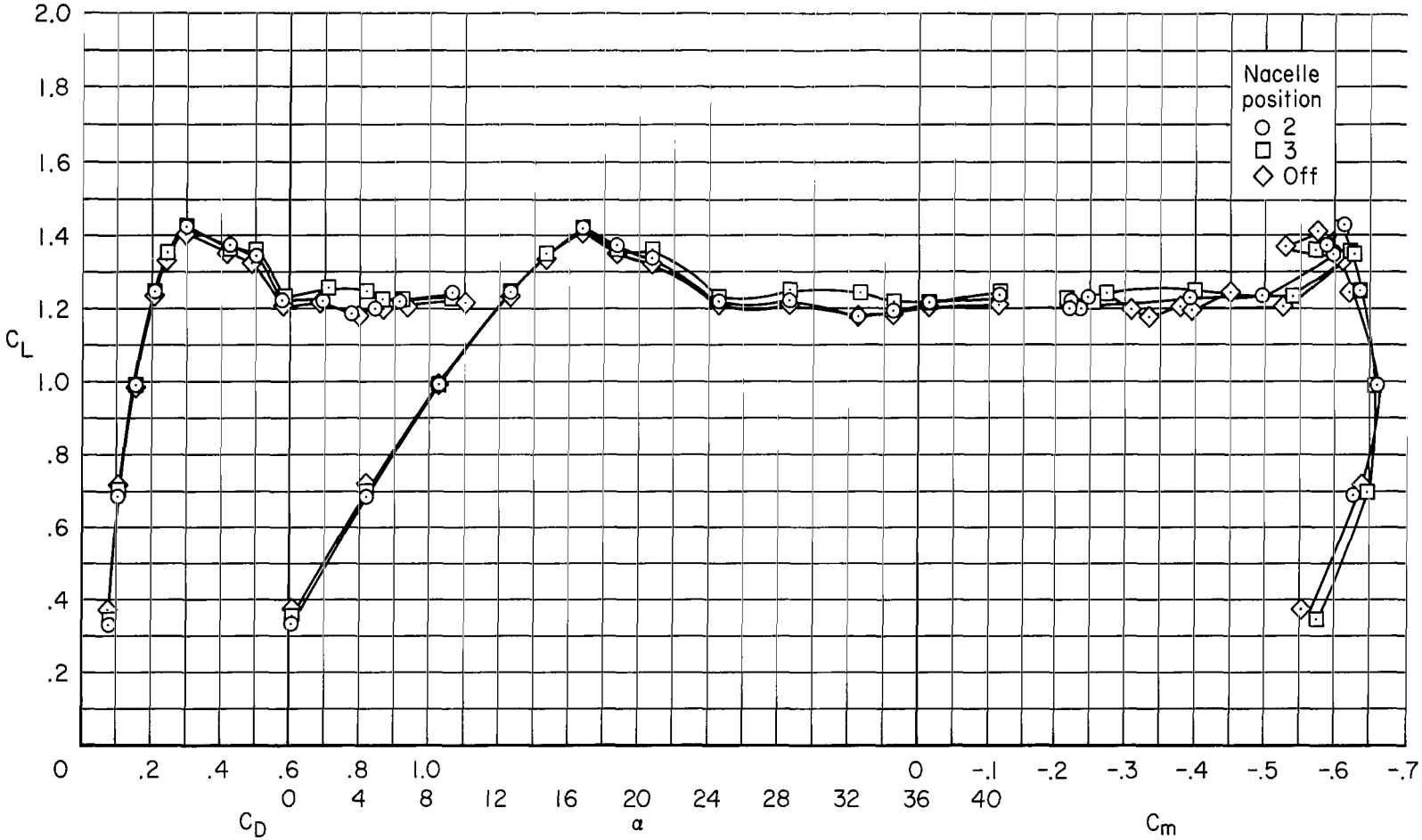

(c) $i_t = 10^\circ$, $\delta_e = 20^\circ$

Figure 12.- Concluded.

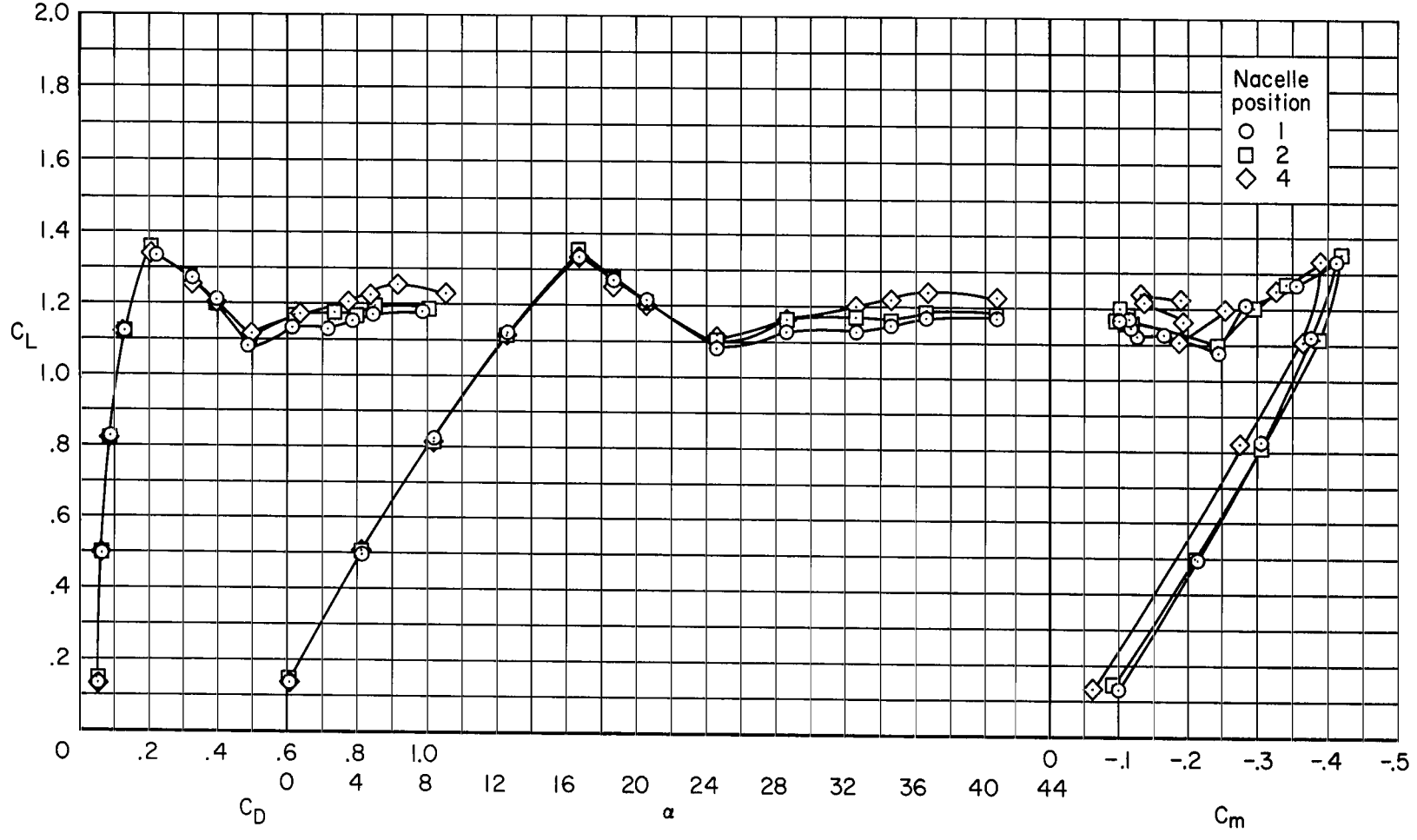

(a) $i_t = -5^\circ$, $\delta_e = 20^\circ$

Figure 13.- Effect of nacelle longitudinal position on the longitudinal characteristics of the model; $\delta_f = 0^\circ$.

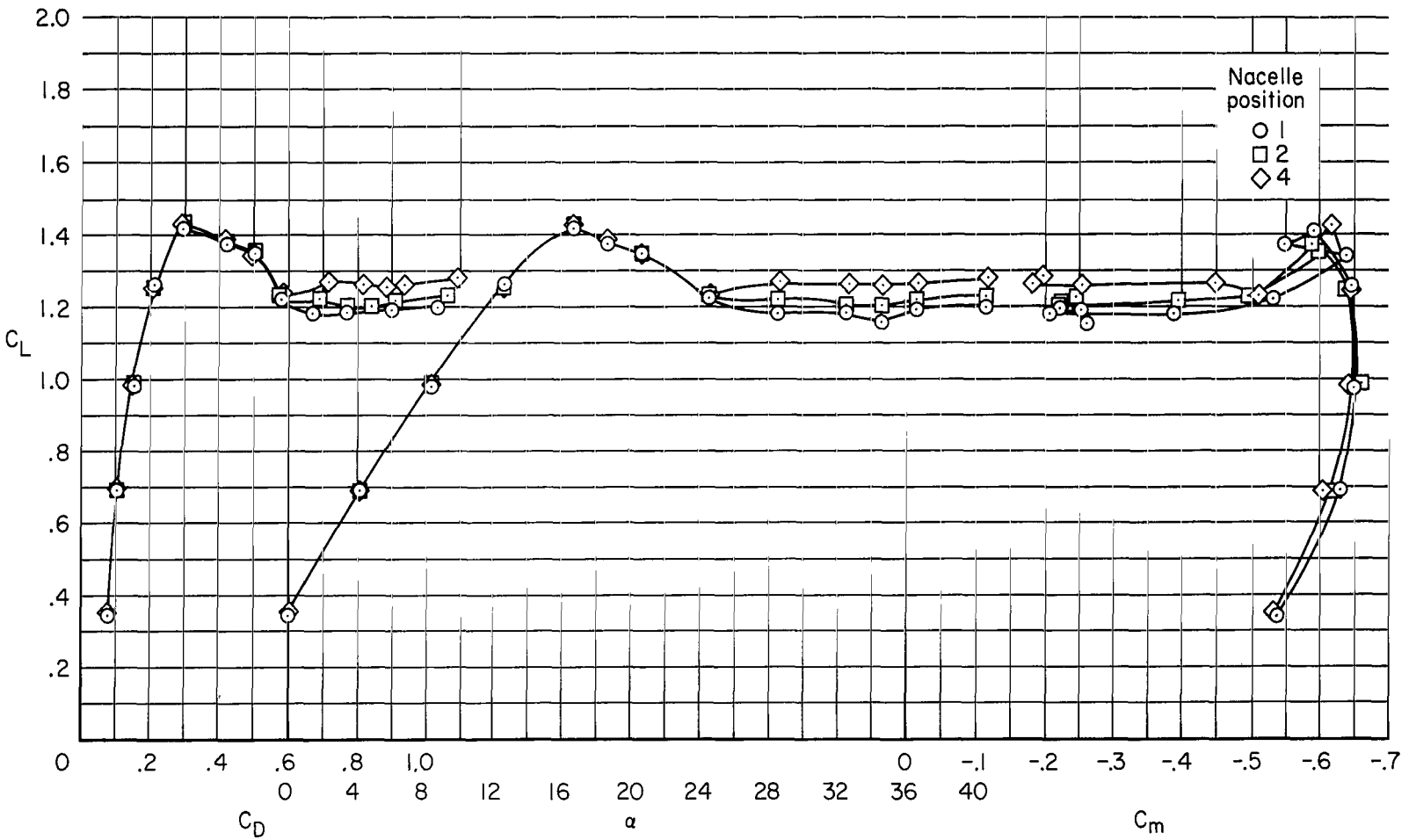

(b) $i_t = 10^\circ$, $\delta_e = 20^\circ$

Figure 13.- Concluded.

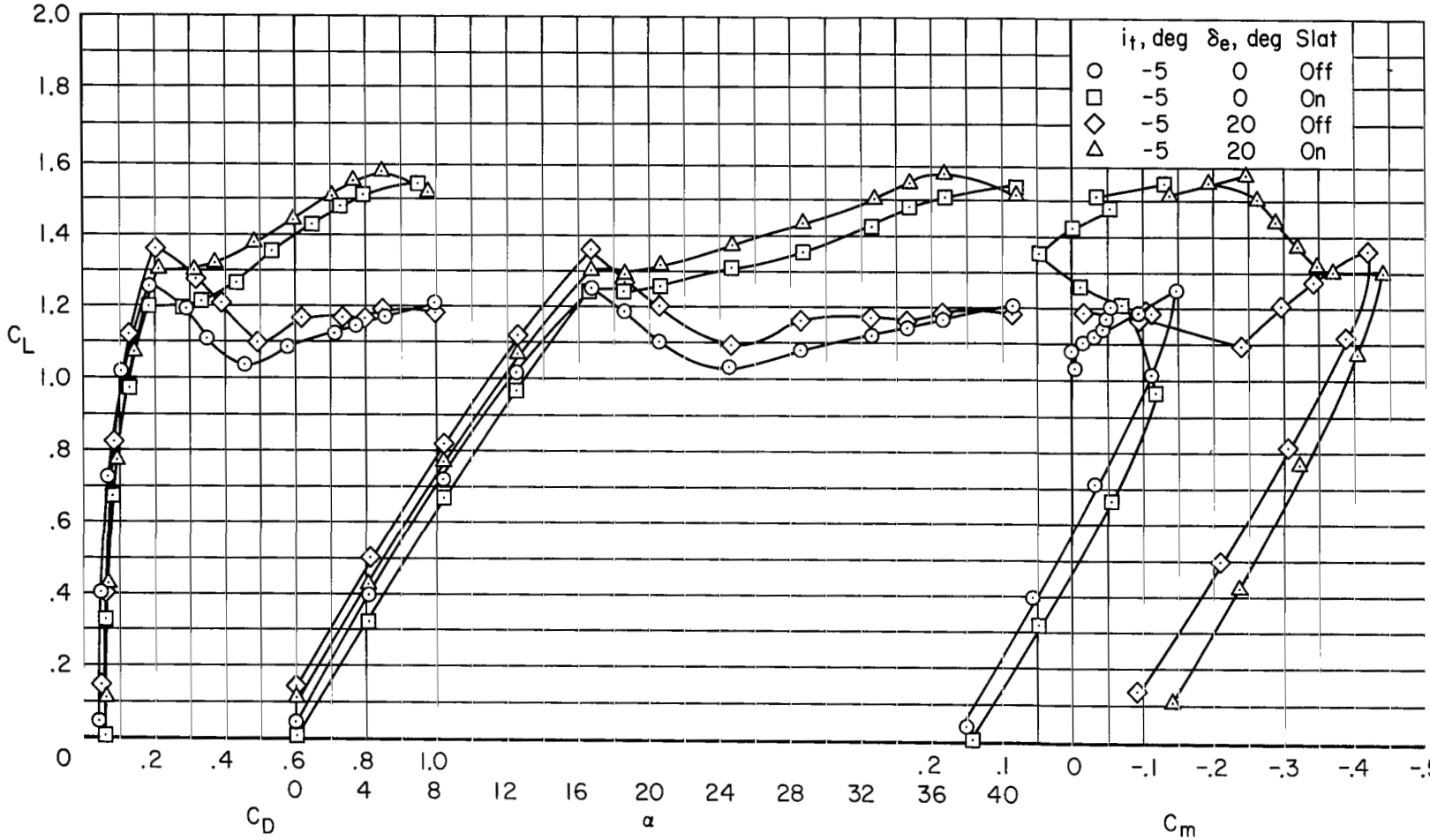

Figure 14.- Effect of half-span inboard leading-edge slats on the longitudinal characteristics of the model; $\delta_f = 0^\circ$, nacelle position 2.

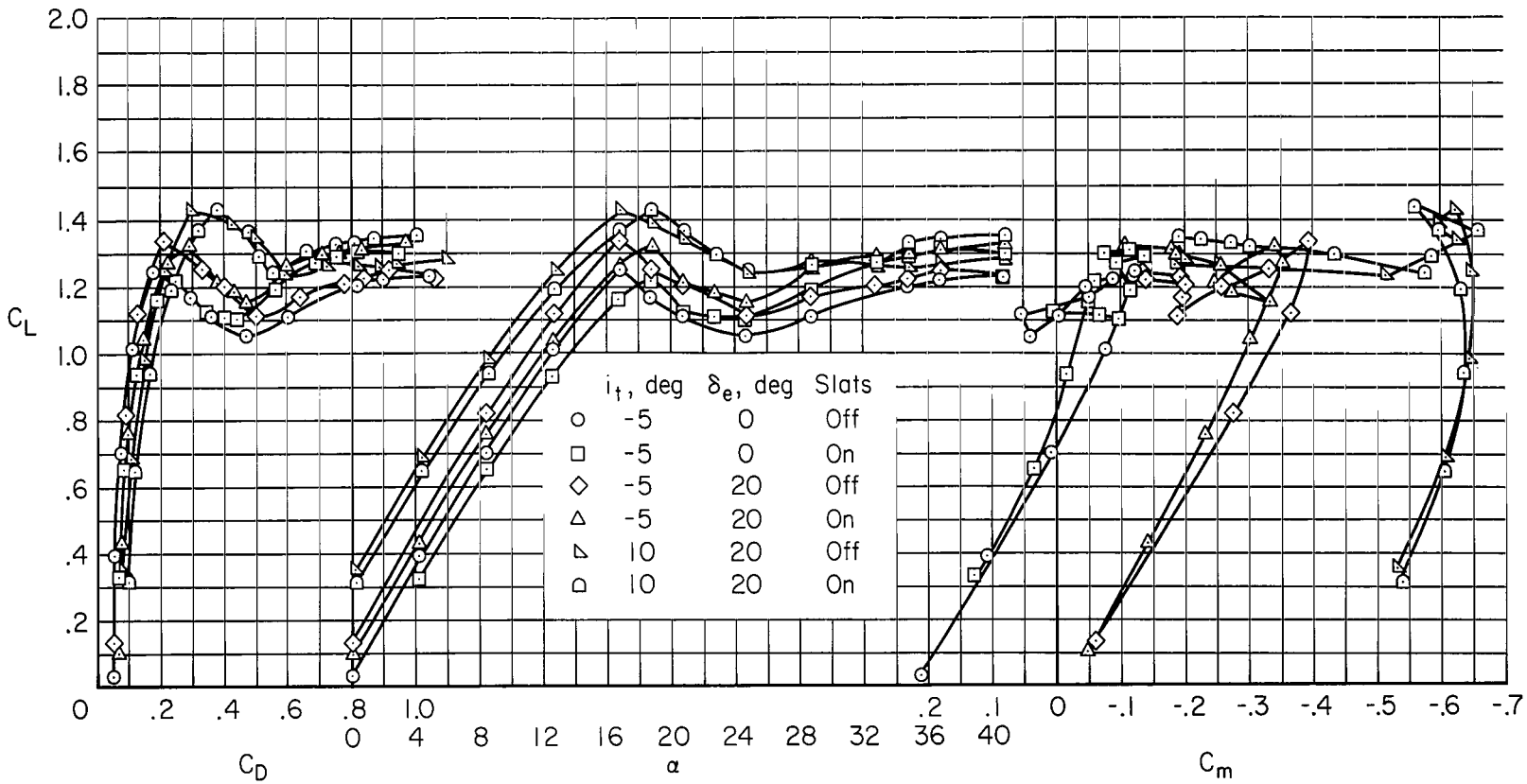

Figure 15.- Effect of half-span outboard leading-edge slats on the longitudinal characteristics of the model; $\delta_f = 0^o$, nacelle position 4.

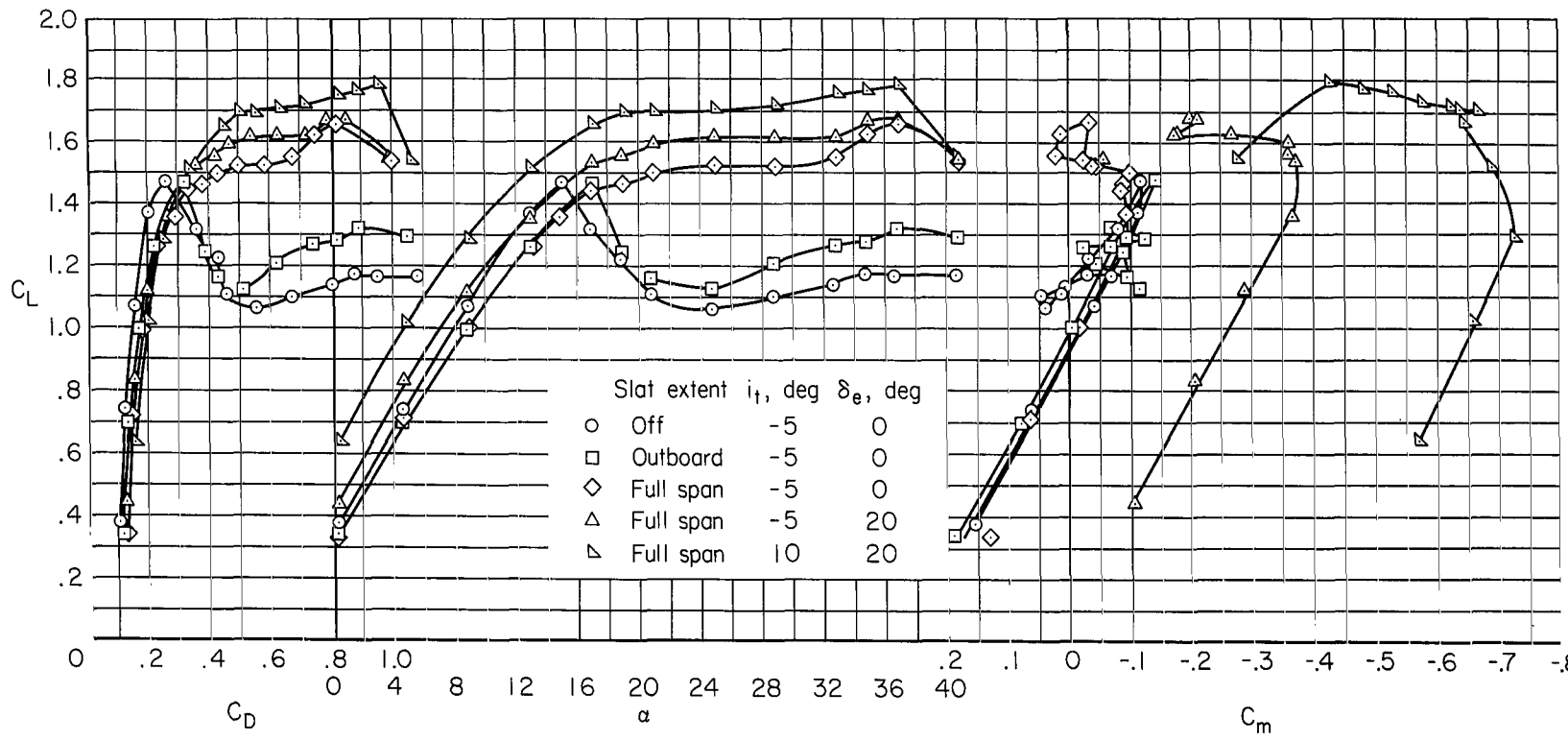

Figure 16.- Effect of leading-edge slats with trailing-edge flap deflected 40° on the longitudinal characteristics of the model; nacelle position 2.

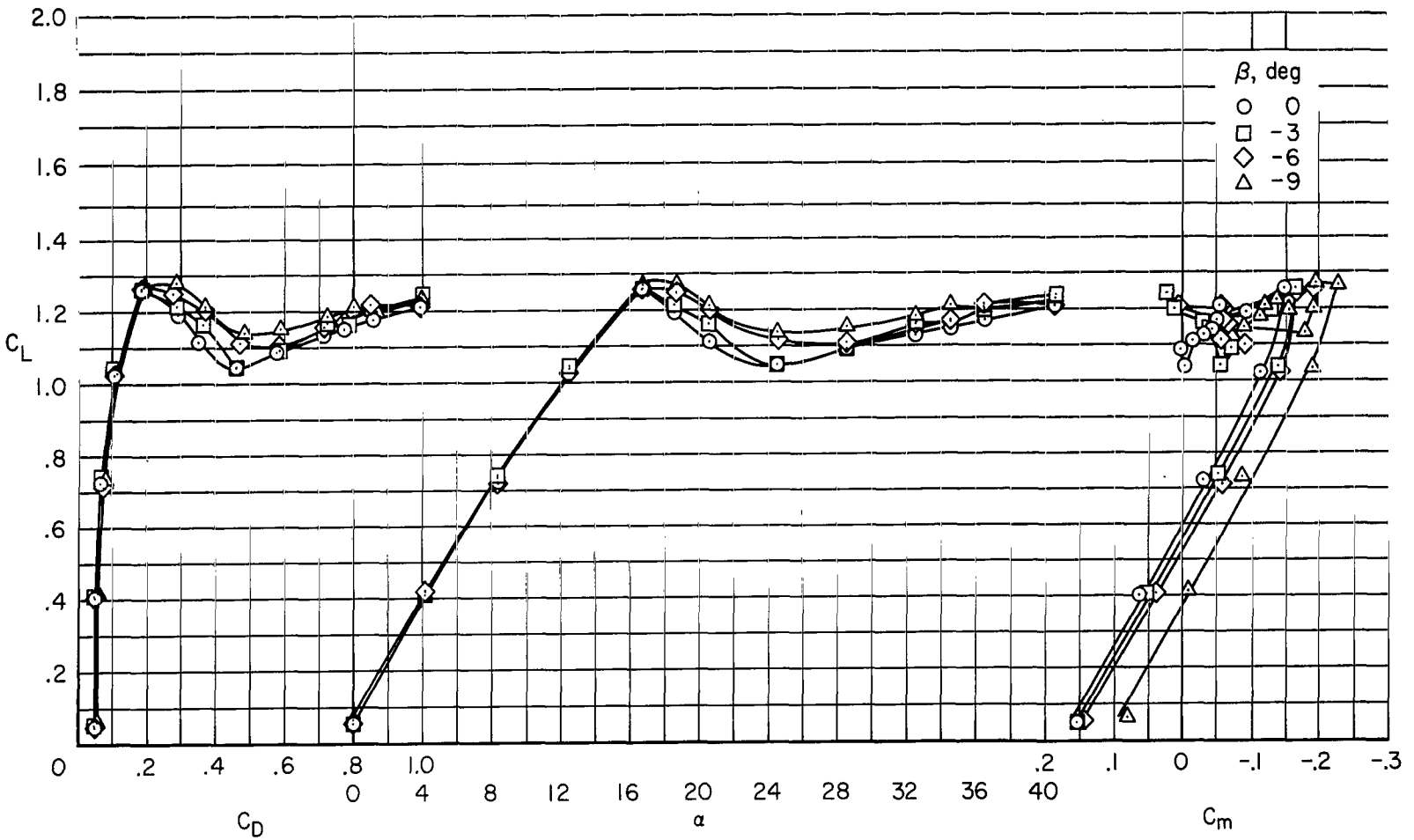

Figure 17.- Effect of sideslip angle on the longitudinal characteristics of the model; $\delta_f = 0^\circ$, nacelle position 2, $i_t = -5^\circ$. $\delta_e = 0^\circ$.

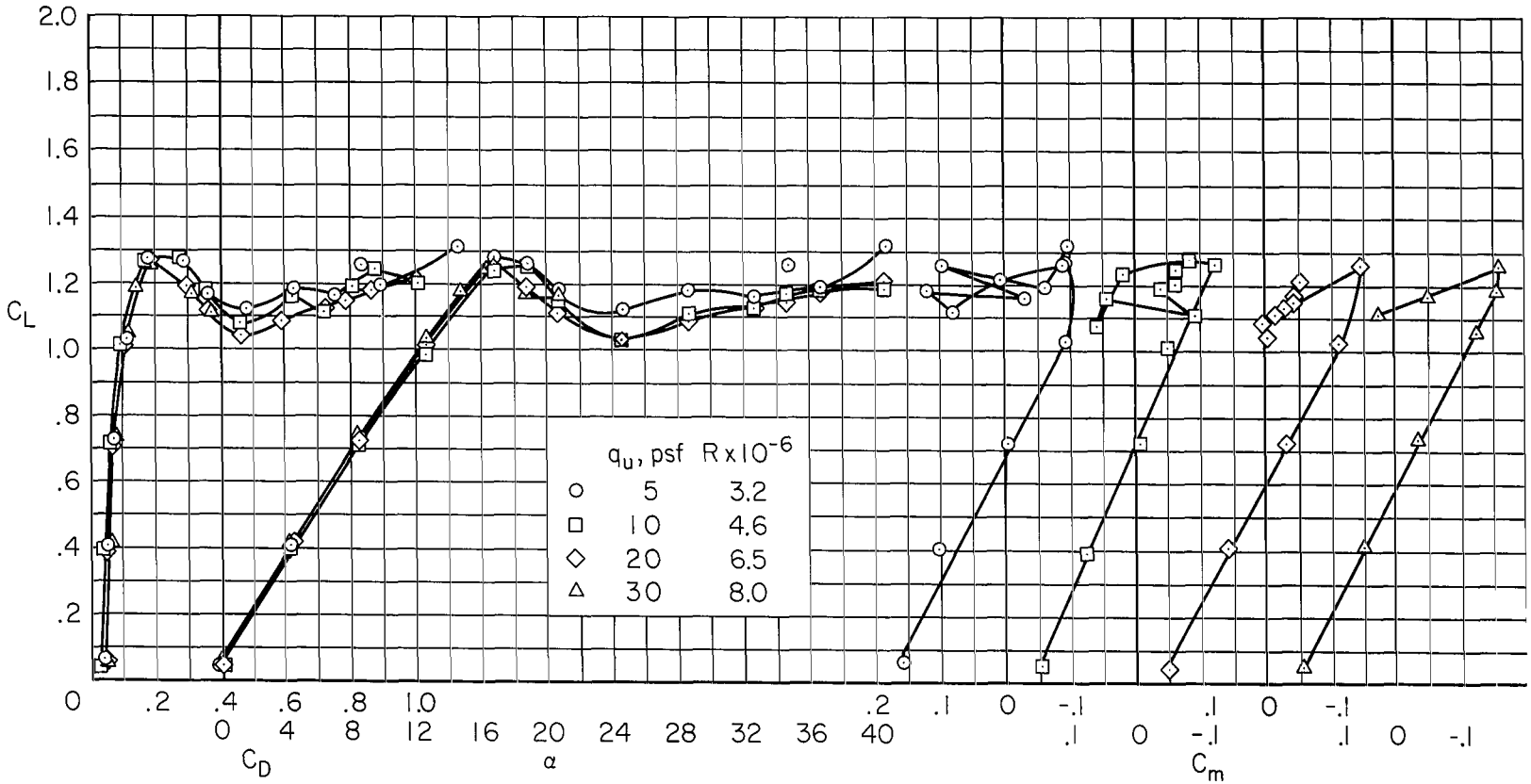

(a) $i_t = -5^\circ$, $\delta_e = 0^\circ$, nacelle position 2.

Figure 18.- Effect of Reynolds number on the longitudinal characteristics of the model; $\delta_f = 0^\circ$.

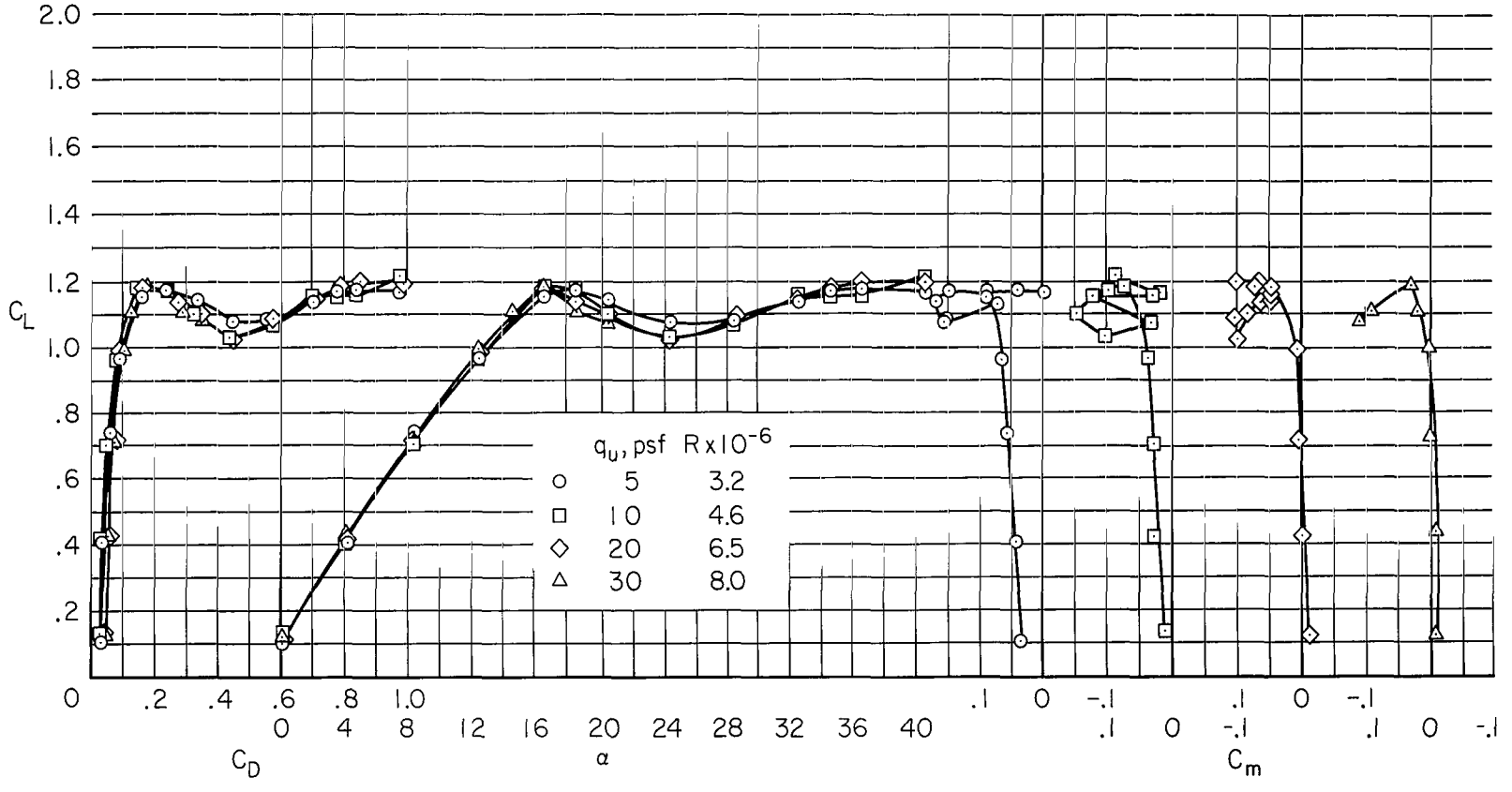

(b) Horizontal tail off, nacelle position 2.

Figure 18.- Continued.

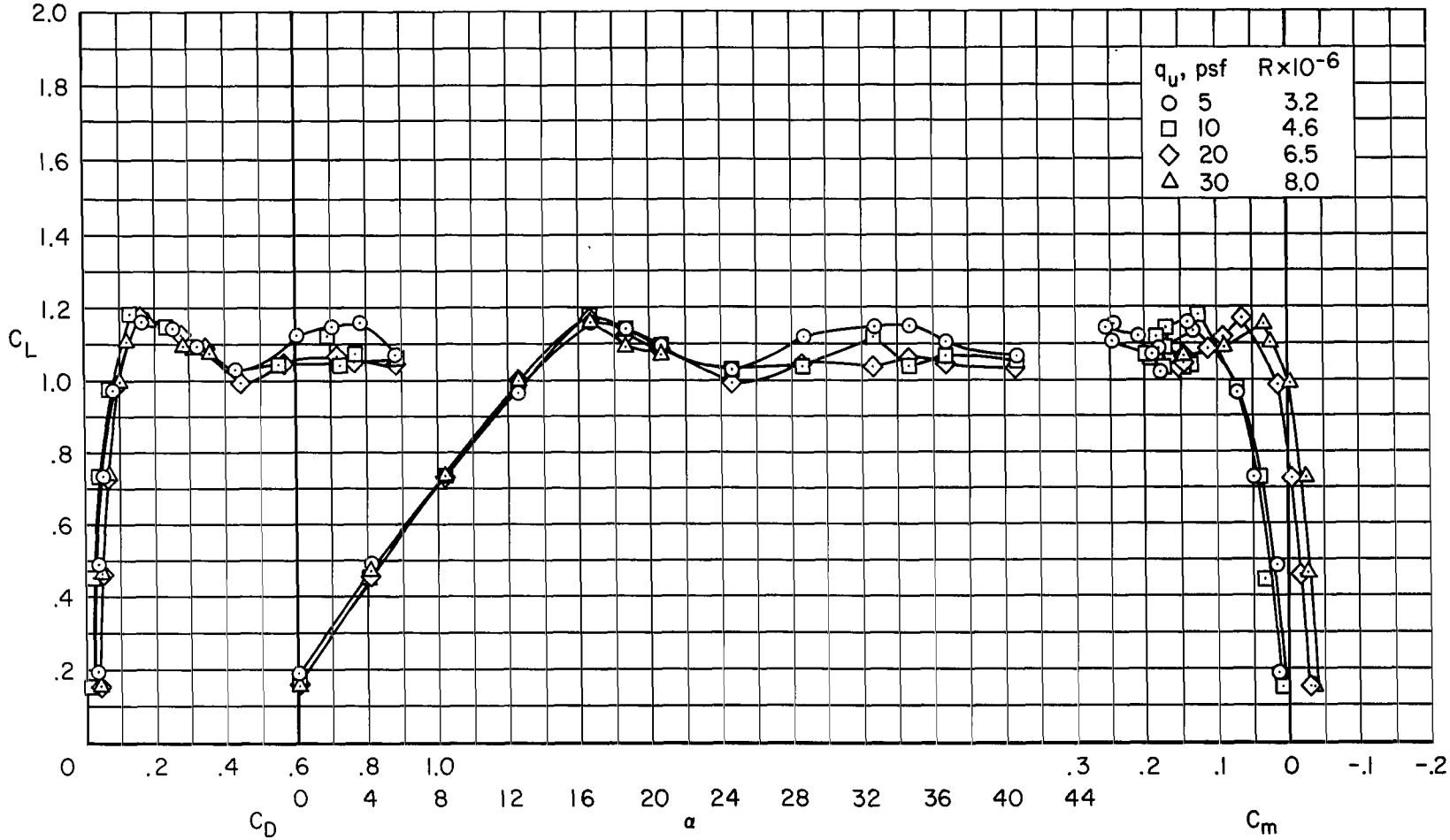

(c) Horizontal tail and nacelles off.

Figure 18.- Concluded.

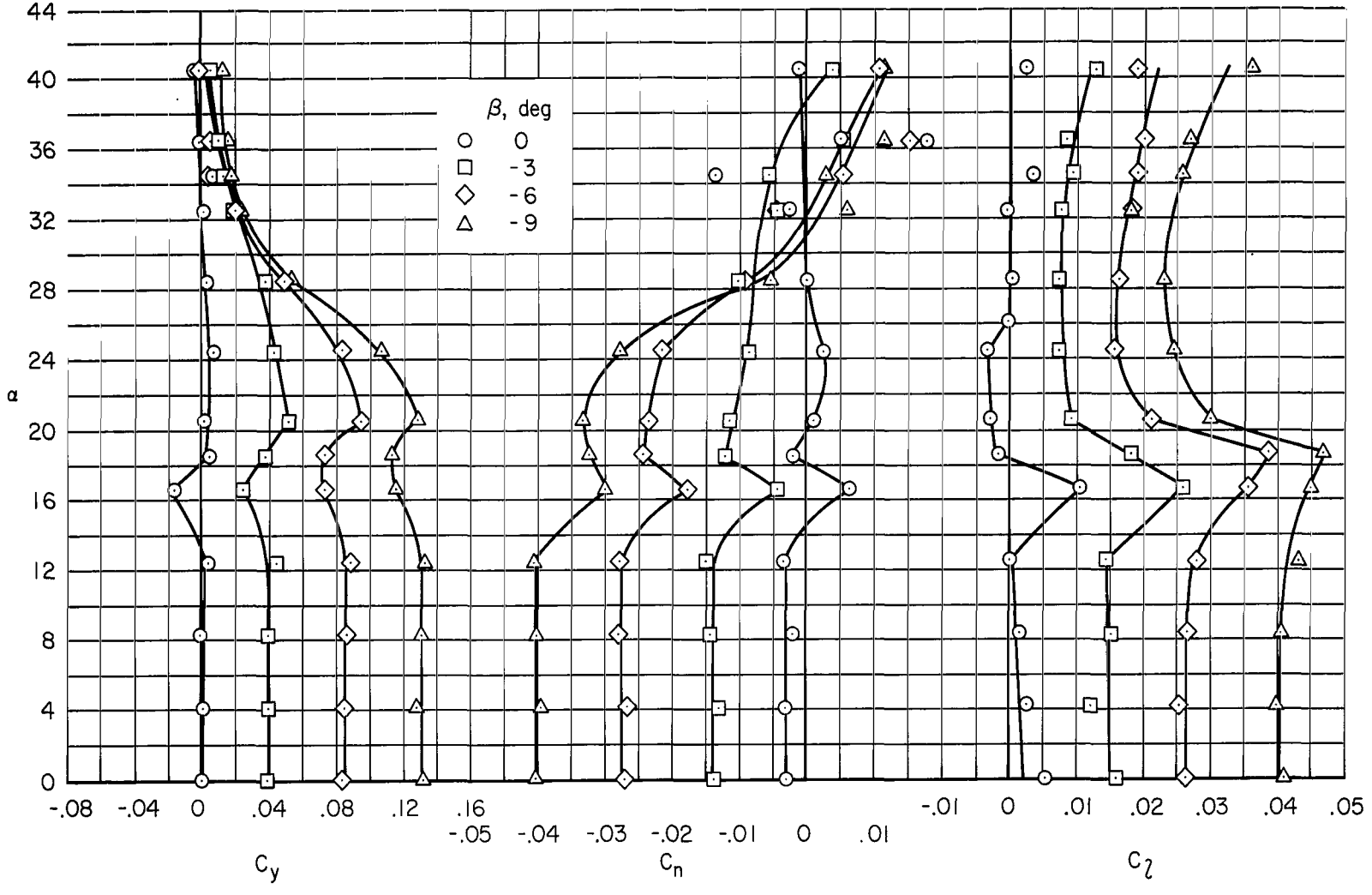

Figure 19.- Effect of sideslip angle on the variation of side force, yawing, and rolling moment coefficients with angle of attack; nacelle position 2, $i_t = -5^\circ$, $\delta_e = 0^\circ$.

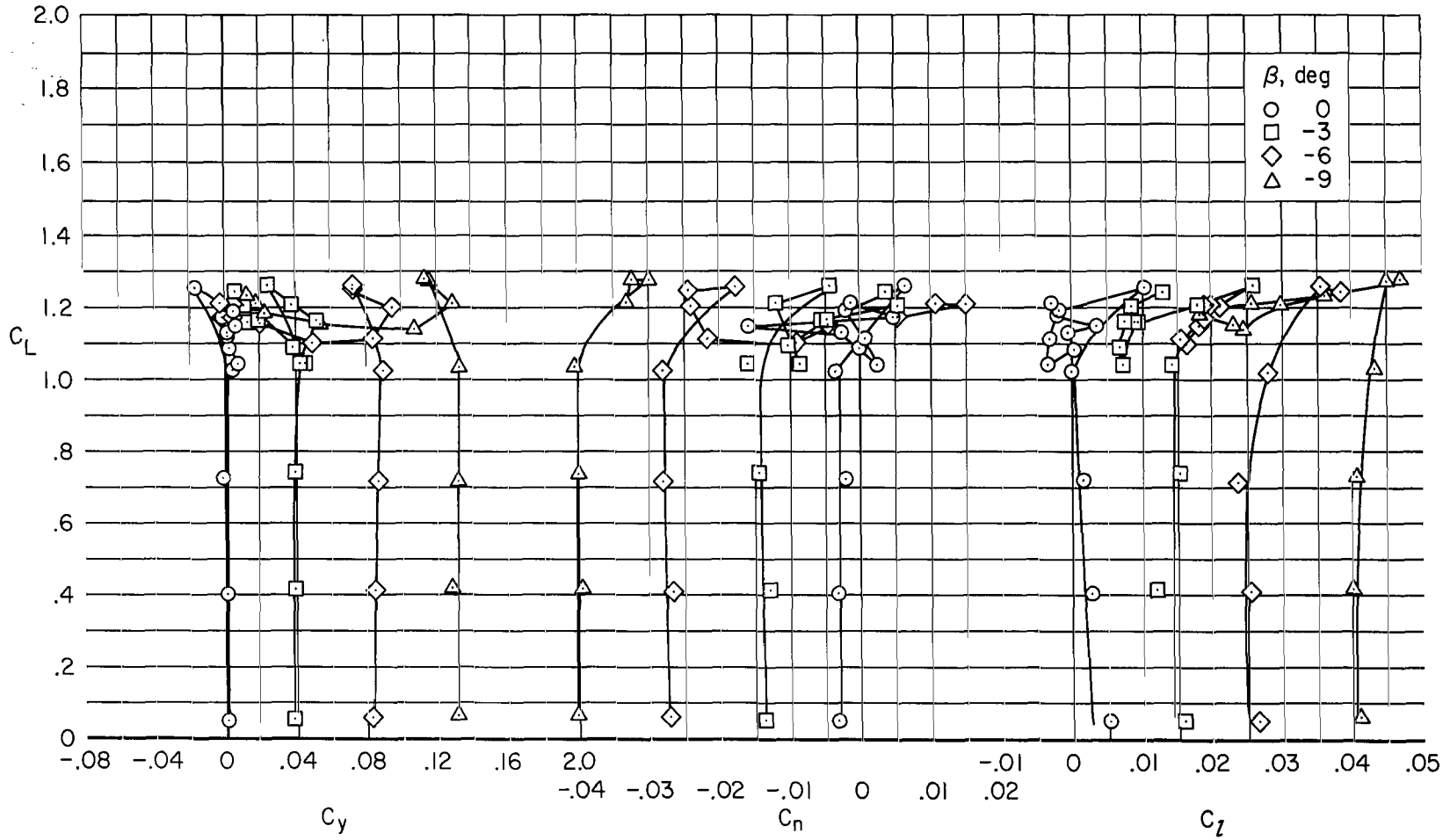

Figure 20.- Effect of sideslip angle on the lateral characteristics of the model; $\delta_f = 0^\circ$, nacelle position 2, $i_t = -5^\circ$, $\delta_e = 0^\circ$.

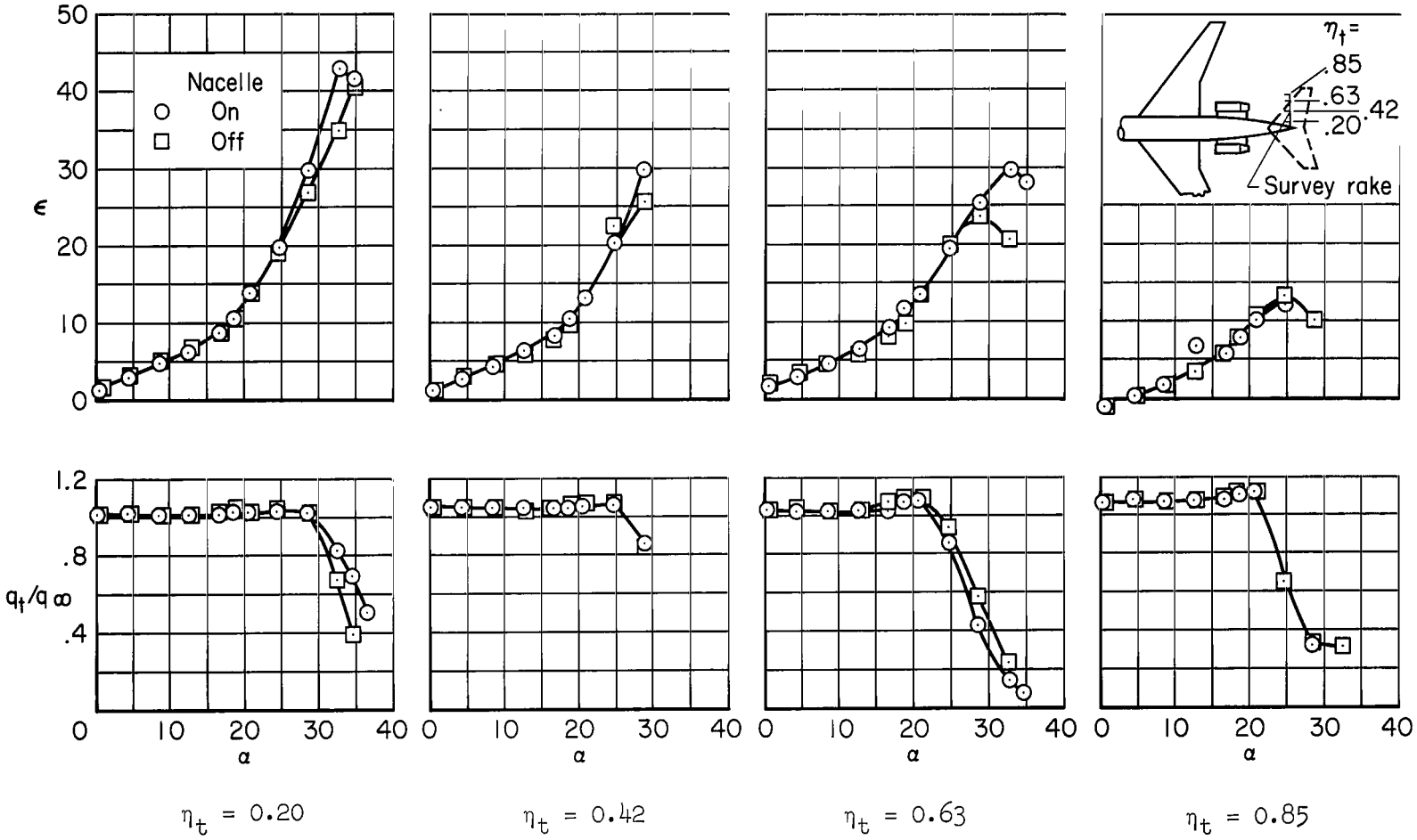

(a) $\delta_f = 0^\circ$

Figure 21.- Effect of nacelle on downwash angle and dynamic pressure ratio at the horizontal tail plane location; tail off, nacelle position 2.

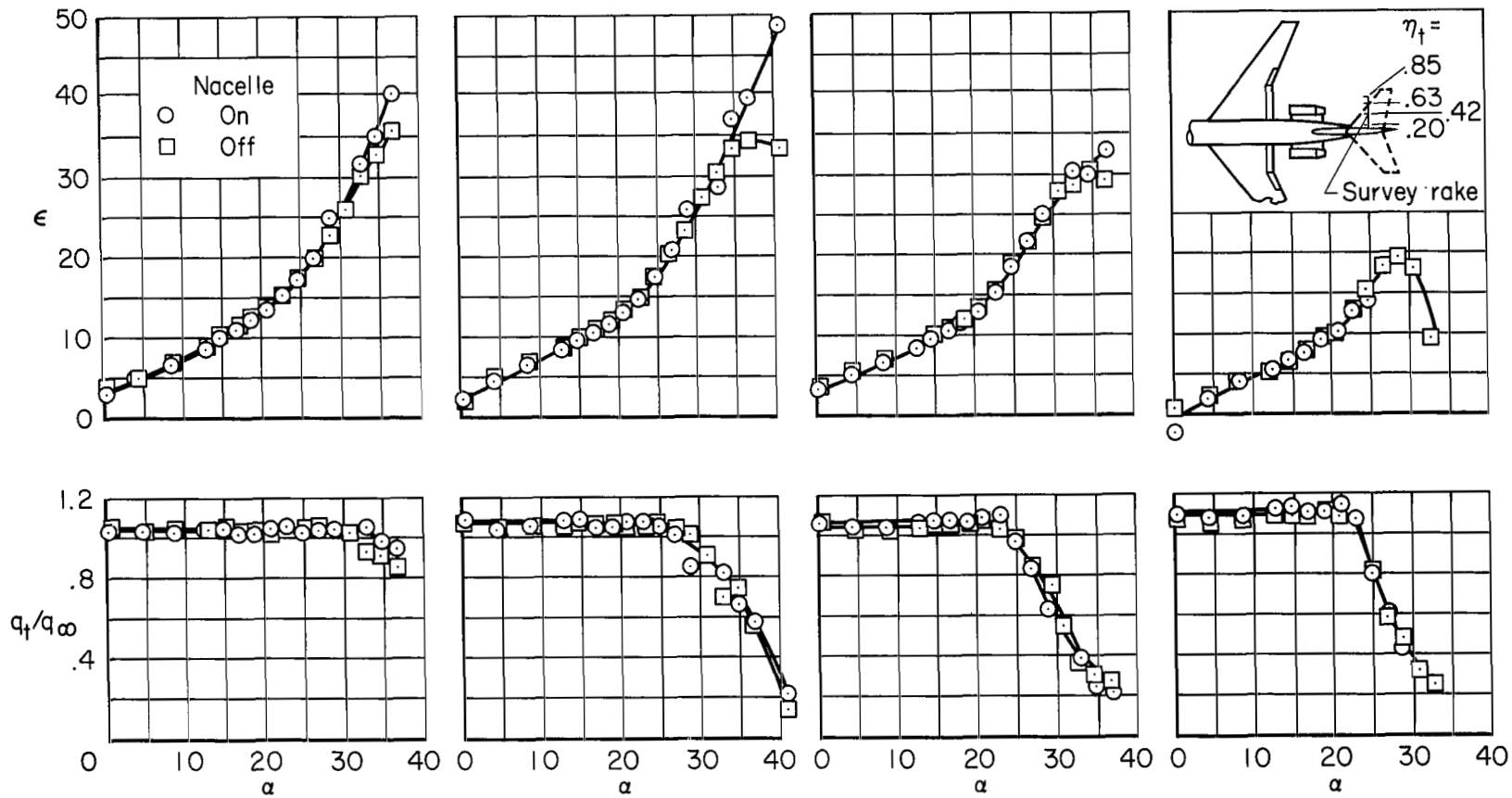

(b) $\delta_f = 40^\circ$, full-span leading-edge slats.

Figure 21.- Concluded.

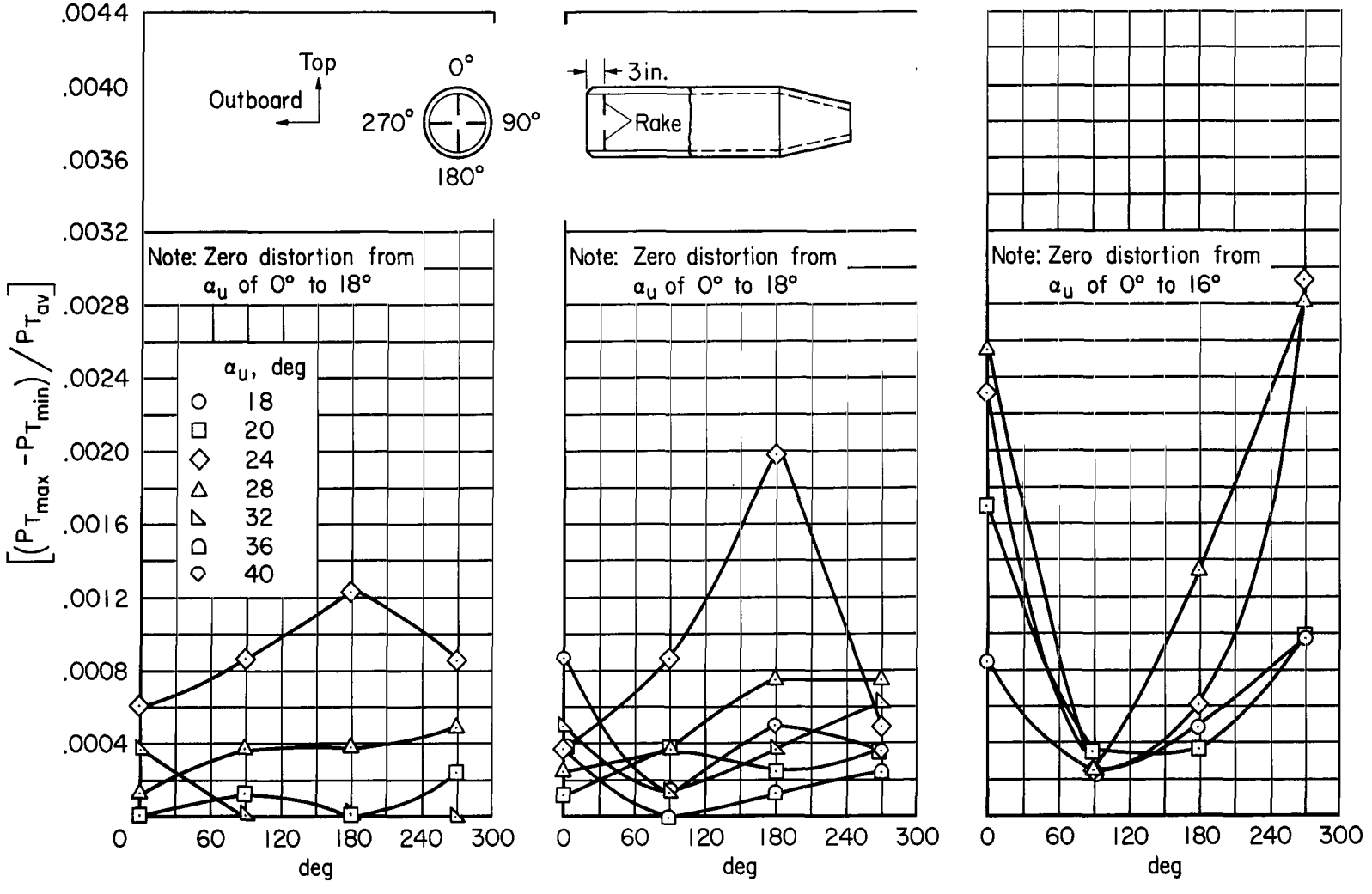

(a) Nacelle position 1, $i_t = -5^\circ$. $\delta_e = 0^\circ$.

(b) Nacelle position 2, $i_t = -5^\circ$, $\delta_e = 0^\circ$.

(c) Nacelle position 4, $i_t = 10^\circ$, $\delta_e = 20^\circ$.

Figure 22.- Effect of nacelle longitudinal position on the nacelle inlet total pressure distortion; $\delta_f = 0^\circ$.

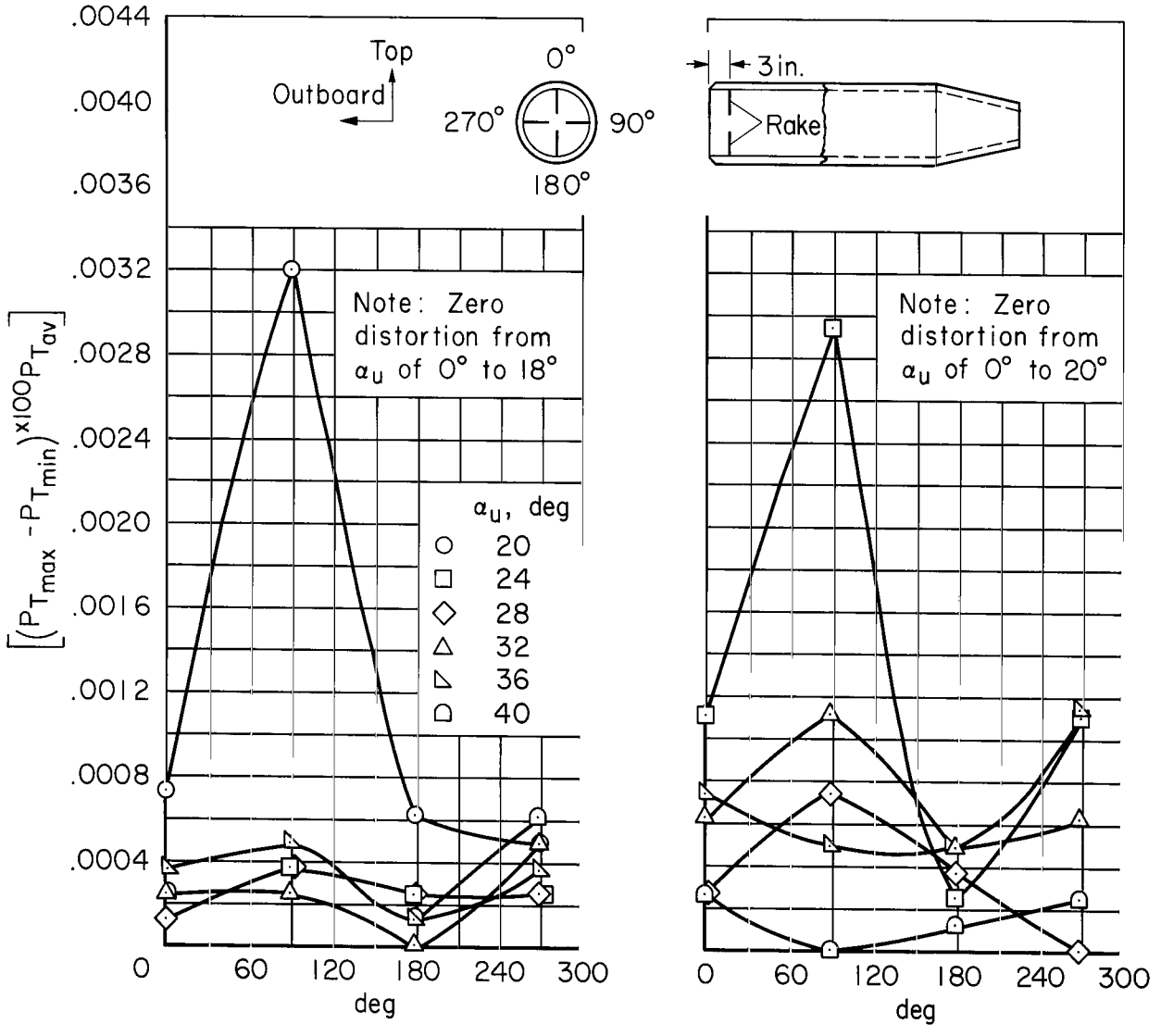

(a) Slats off.

(b) Full-span slats.

Figure 23.- Effect of leading-edge slats with trailing-edge flaps deflected 40° on the nacelle inlet total pressure distortion; nacelle position 2, $i_t = -5^\circ$, $\delta_e = 0^\circ$.

"The aeronautical and space activities of the United States shall be conducted so as to contribute . . . to the expansion of human knowledge of phenomena in the atmosphere and space. The Administration shall provide for the widest practicable and appropriate dissemination of information concerning its activities and the results thereof."

—NATIONAL AERONAUTICS AND SPACE ACT OF 1958

NASA SCIENTIFIC AND TECHNICAL PUBLICATIONS

TECHNICAL REPORTS: Scientific and technical information considered important, complete, and a lasting contribution to existing knowledge.

TECHNICAL NOTES: Information less broad in scope but nevertheless of importance as a contribution to existing knowledge.

TECHNICAL MEMORANDUMS: Information receiving limited distribution because of preliminary data, security classification, or other reasons.

CONTRACTOR REPORTS: Technical information generated in connection with a NASA contract or grant and released under NASA auspices.

TECHNICAL TRANSLATIONS: Information published in a foreign language considered to merit NASA distribution in English.

TECHNICAL REPRINTS: Information derived from NASA activities and initially published in the form of journal articles.

SPECIAL PUBLICATIONS: Information derived from or of value to NASA activities but not necessarily reporting the results of individual NASA-programmed scientific efforts. Publications include conference proceedings, monographs, data compilations, handbooks, sourcebooks, and special bibliographies.

Details on the availability of these publications may be obtained from:

SCIENTIFIC AND TECHNICAL INFORMATION DIVISION

NATIONAL AERONAUTICS AND SPACE ADMINISTRATION

Washington, D.C. 20546